

Spatial heterodyne spectrometer. Feasibility study for space applications.

Auteur : Schlembach, Leo

Promoteur(s) : Habraken, Serge

Faculté : Faculté des Sciences

Diplôme : Master en sciences spatiales, à finalité spécialisée

Année académique : 2020-2021

URI/URL : <http://hdl.handle.net/2268.2/11280>

Avertissement à l'attention des usagers :

Tous les documents placés en accès ouvert sur le site le site MatheO sont protégés par le droit d'auteur. Conformément aux principes énoncés par la "Budapest Open Access Initiative"(BOAI, 2002), l'utilisateur du site peut lire, télécharger, copier, transmettre, imprimer, chercher ou faire un lien vers le texte intégral de ces documents, les disséquer pour les indexer, s'en servir de données pour un logiciel, ou s'en servir à toute autre fin légale (ou prévue par la réglementation relative au droit d'auteur). Toute utilisation du document à des fins commerciales est strictement interdite.

Par ailleurs, l'utilisateur s'engage à respecter les droits moraux de l'auteur, principalement le droit à l'intégrité de l'oeuvre et le droit de paternité et ce dans toute utilisation que l'utilisateur entreprend. Ainsi, à titre d'exemple, lorsqu'il reproduira un document par extrait ou dans son intégralité, l'utilisateur citera de manière complète les sources telles que mentionnées ci-dessus. Toute utilisation non explicitement autorisée ci-avant (telle que par exemple, la modification du document ou son résumé) nécessite l'autorisation préalable et expresse des auteurs ou de leurs ayants droit.



SMEM0029-1

Master Thesis

Spatial Heterodyne Spectrometer
Feasibility Study for Space Applications

Promoter:

HABRAKEN Serge

SCHLEMBACH Leo

Readers:

LOÏQ Jérôme

HUBERT Benoît

FLEURY-FRENETTE Karl

Academic year 2019-2020 (extended session: January 2021)



SMEM0029-1

Master Thesis

Spatial Heterodyne Spectrometer
Feasibility Study for Space Applications

accepted by:

HABRAKEN Serge

LOÏQ Jérôme

SCHLEMBACH Leo

HUBERT Benoît

FLEURY-FRENETTE Karl

Abstract

This work is about the study of the feasibility of a miniaturized SHS (Spatial heterodyne spectrometer), in order to see, if it is possible to mount it in CubeSat's. It has been done with the help of Pr. Serge Habraken, who is member of CSL.

The advantage of a SHS on other spectrometers such as Fabry-Perot is that it doesn't need any moving part, whatever the bandwidth it is designed for.

Another advantage is the possibility to conserve a large field of view, even with a good spectral resolution.

However, contrary to the double scale gratings, SHS need some calculation to reconvert the recorded signal (on the detector) into spectral data. That can be done with Fourier transforms that are relatively easy to model with Matlab.

Two cases are studied in this work: one with a smooth but noisy shaped spectrum (based on Doppler shift in a spectral line in a quasar), and another based on narrow spectral lines (based on the study of water absorption lines in the martian atmosphere).

The feasibility of both cases ensures the feasibility of more general cases, since it consist after all of superposition of two behaviours.

The level of detail goes up to the thermal considerations for the spectral lines. However, in our case, we neglect in this work the treatment of wavenumber dependent shifts, so that, as we will see, the recovered spectrum, even if the general shape is similar to the input spectrum, will be slightly distorted.

Acknowledgements

The first persons, I want to mention are my parents, who during those long years supported me mentally and financially, so that I could be able to be here and present this thesis.

After my parents, I would like to thank all the professors of the AGO department, especially Pr. Serge Habraken, who never ceased to believe in me, despite the time it took to me to arrive at the end of my cursus.

I Also want to mention Pr. Philippe Lejeune (AgroBiotech Gembloux), who supervised my stage in 2019. He and his team brought me a precious experience, that I would like to take advantage of.

I would like to thank the ASH team, the personal of th psychiatric unit in Hospital St Josef, Sankt Vith, the Cral, as well as some friends I met in Sankt Vith. I'd like to mention especially Florence Elleboudt, Lygia Leyendecker, Marie-Christine Wetzels and Lisa Jansana.

Finally, mens sana in corpore sano, I want to thank the members of the Royal Sport Nautique de Liège who helped me when I had depressive moments or during my panic attacks.

Contents

	Introduction	1
1	Context and Tools	2
1.1	Context	2
1.2	Tools	3
2	Theory	4
2.1	Grating and Littrow Angle	4
2.2	Michelson Interferometer	5
2.3	Application to the SHS	6
2.4	Parameterisation	9
2.4.1	Simulation	9
2.4.2	Discussion	10
3	Comparison with other Spectrometers	12
3.1	Fabry-Perot Interferometer	12
3.2	Michelson interferometer	14
3.3	Scale grating	14
4	Space Applications	15
4.1	Chemical Sounding of the Atmosphere	15
4.1.1	Limb Sounding of the Atmosphere	15
4.1.2	Pollutant survey of the Atmosphere using Raman Spectroscopy	16
4.1.3	Water content study of the Martian Atmosphere	17
4.2	In Situ Sounding	17
4.2.1	Mineral study of Meteorites, Comets and other Objects with Raman Spectroscopy	17
4.2.2	LIBS	18
4.3	Redshift measurements	18

5	Spectrum Recovery	20
5.1	Detector Signal	21
5.1.1	Ideal Spectrometer	21
5.1.2	Ideal Image of a Delta Function Spectrum	22
5.1.3	Ideal image for the Filter function	22
5.1.4	Recovery of the input spectrum	23
6	Signal processing for Applications	25
6.1	Device dimensions	25
6.2	Doppler Shift in Quasar Disks	27
6.2.1	System Parameters	27
6.2.2	General Processing Algorithm	28
6.2.3	Flat Field Correction	29
6.2.4	Corrections due to Errors on Wavelength Measurements	29
6.2.5	Phase Shift Correction	30
6.3	Mars Atmospheric Water Lines	31
6.3.1	System Parameters	31
6.3.2	General Processing Algorithm	32
6.3.3	Thermal Considerations	33
6.3.4	Calibration of the Recovered Spectrum	34
6.3.5	Noise	35
6.4	Spectrum Recovery	37
6.5	Summary and Results	37
6.5.1	Doppler Shift in Quasar Disks	39
6.5.2	Mars Atmospheric Water Lines	41

Conclusions **44**

Introduction

A dispersive spectrometer is a device, that separates the light into all its frequencies. To analyze the spectrum, with such a device, one must use, in addition to the prism (or any other dispersion device), a slit, in order to select the desired frequency.

By opposition to a dispersive spectrometer, a Fourier transform spectrometer will not separate the components of the light. It will be based on superposition of all the components of the light input, each one of the components being characterized with a pattern. The output will be the convolution of the input signal with the frequency-dependent pattern. To analyze the spectrum, one must deconvolve the output signal.

While for the dispersive spectrometers, the accuracy of the measure is related to the width of the slit, for the Fourier transform spectrometer, one can reach in theory, an infinite resolution. However, since the detectors are not infinite planes, it will be, in practice, limited by the size of the detector.

Furthermore, the pixel size will also affect the resolution, by the fact that it will determine the maximum bandwidth.

An example of a Fourier transform spectrometer is the spatial heterodyne spectrometer (SHS). It is based on a Michelson interferometer, modified in such a way that the mirrors are replaced by gratings or, for a more compact version, by grisms. The orientation of the gratings are determined by the excitation wavelength (or threshold frequency), at which, the desired angle between incoming and outgoing beam must be zero. For all other wavelengths, the angle formed between incoming and outgoing wavefronts will result in an optical path difference between the fronts coming from both gratings, depending on the position of the observer. This will result in fringes on the detector. Simulations using MATLAB will be done for several exciting wavelengths, as well as several pixel sizes and detector sizes. The results will be plotted on $\delta\lambda$ - δx graphs and tables will summarize the results.

Finally, applications relative to the space industry will be considered.

Chapter 1

Context and Tools

1.1 Context

Space optics is a topic at the intersection between space sciences and space engineering. For this reason, in the frame of a master thesis in space sciences with industrial issues, the choice of making a work based on optics seems to be a good approach to prepare for the professional life.

The SHS are very demanding technologies, because of their compactness, and the simple manufacturing. Furthermore, they present the advantage to be not limited in illumination by small apertures, in contrary to the dispersive spectrometers. For this reason, it can be interesting to study such a device, because of its possible applications to the space industry. For the work itself, the goal will be to acquire and develop skills that will allow to enter the world of industry. This will also involve basic programming skills (such as the use of MATLAB). The goals to achieve are:

- Make a mathematical model of the spectrometer
- Make simulations for different configurations
- Consider space applications

The thesis should provide feasibility information for space applications related to the SHS. For the dispersive part of the spectrometer, we will consider the grating.

We will also keep in mind the fact, that the SHS should fit in a one unit Cube Sat. Taking in consideration the propulsion, the attitude control and the power device, the full volume is not entirely dedicated to the payload. The structure and the reaction wheels can fit in a one cm thick shell. This leaves us with a $8 \times 8 \times 8 \text{cm}^3$ volume. The thrusters can be places on the corners of the spacecraft and fit in a $2 \times 2 \times 2 \text{cm}^3$ cube. This leaves us for the thermal control, communication systems, power devices, detectors and optical devices with a volume of $8 \times 8 \times 8 \text{cm}^3$. Considering

that the full length can be used for the optical and detection devices, we should have a SHS that fits in $6 \times 4 \times 4 \text{cm}^3$ block. Taking into account the structure of the optical device and the focusing systems, we will assume that the grating have a 25mm width. This can leave us with a margin and will allow to fit the other components of the spacecraft.

1.2 Tools

The courses of instrumental optics, space optics and space observation gave all the physics tools to understand the physical principles of the SHS. This includes the use of Fourier transform. The course of introduction to the numerical methods (at UCLouvain) was dedicated to the basics of MATLAB. For longer works, it will be useful to treat with customized functions (in order to make the code less heavy).

A bibliographic research will complete the skills acquired in the frame of these courses. Finally, regular meetings with the thesis supervisor will provide responses to eventual questions as well as guidelines for the progression of the work.

Chapter 2

Theory

2.1 Grating and Littrow Angle

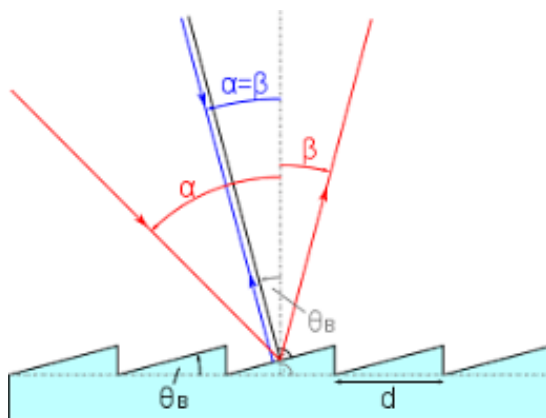


Figure 2.1: Blazed grating: the angle for which incident and reflected light are coincident is called Littrow angle. This angle is associated with a specific wavelength

A grating is an optical device that consists in a reflective surface with blazed grooves spaced each other by a distance d . Due to the grooves, the components of the light will interfere each other after reflection. The result is a reflection of the light in a direction depending of the wavelength.

The reflection law for a grating of groove spacing d is given by the following formula:

$$d(\sin\alpha + \sin\beta) = m\lambda \quad (2.1)$$

In the equation, α and β are respectively incident and reflected angles and m is the diffraction order. If we take the first order of diffraction, given a wavelength λ_0 , we find an angle for which reflected and incident angles are the same. This angle is called Littrow angle. It will also

correspond to the blazing angle for the grooves:

$$\Theta_B = \arcsin\left(\frac{\lambda_0}{2d}\right) \quad (2.2)$$

For the simplest configuration of the SHS, this is also the angle formed by the grating and the incident wavefront (i.e. the beam splitter). For the rest of the discussion, we will consider small deviations from the excitation wavelength.

We can already see a first condition on the groove density of the grating, because the sine must be lower than one, i.e.:

$$\lambda_0 < 2d \quad (2.3)$$

2.2 Michelson Interferometer

Let's consider a plane wave that is reflected on a grating in the SHS. If the wavelength differs from the excitation wavelength by an amount $\delta\lambda$, it will quit the grating with an angle in respect to the incident wavefront of α . Hence, on the focal plane, we will have two plane waves forming an angle of 2α . Let's study the fringe pattern formed by two plane waves separated by an angle 2α . For this purpose, we must consider the Plane wave expressed in terms of electromagnetic field:

$$\begin{aligned} \vec{E} &= \vec{E}_1 + \vec{E}_2 \\ \text{with} & \\ \vec{E}_1 &= \vec{E}_0 e^{i(\omega t - \vec{k}_1 \cdot \vec{r})} \\ \vec{E}_2 &= \vec{E}_0 e^{i(\omega t - \vec{k}_2 \cdot \vec{r})} \end{aligned} \quad (2.4)$$

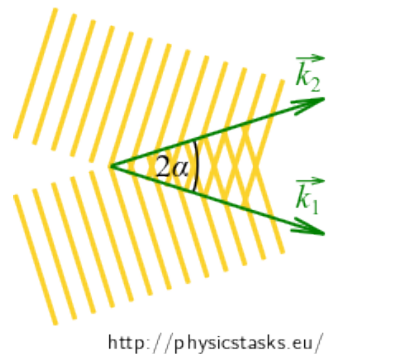


Figure 2.2: Two plane waves interfering. One must make vectorial addition to get the fringe pattern.

The power intensity of the signal is proportional to the square of the norm of the total electromagnetic field. Reminding that \vec{k}_1 and \vec{k}_2 have the same norm and that they form an angle of 2α , and taking as x-axis the axis perpendicular to the sum of the two vectors, we calculate:

$$\begin{aligned}
w_E &= \frac{\epsilon_0}{4} (E_1 \vec{r} + E_2) \cdot (E_1 \vec{r} + E_2)^* \\
&= \frac{\epsilon_0}{4} E_0^2 (1 + e^{i(\vec{k}_2 - \vec{k}_1) \cdot \vec{r}} + e^{-i(\vec{k}_2 - \vec{k}_1) \cdot \vec{r}} + 1) \\
&= \frac{\epsilon_0}{2} E_0^2 (1 + \cos(\vec{r} \cdot (\vec{k}_2 - \vec{k}_1))) \\
&= \frac{\epsilon_0}{2} E_0^2 (1 + \cos(2kx \cdot \sin(\alpha))) \\
&= E_0^2 \epsilon_0 \cos^2(kx \cdot \sin(\alpha))
\end{aligned} \tag{2.5}$$

This is a periodic expression, that is maximum for $x = \frac{N\pi}{k \cdot \sin(\alpha)}$. In this section, k is the wavenumber expressed as $\frac{2\pi}{\lambda}$. For the next part of the discussion, we will consider the quantity $\sigma = \frac{1}{\lambda}$. When we will use k for the wave number, it will also correspond to $\frac{1}{\lambda}$.

Because the reflected light is reflected with an angle of $2\theta_L + \delta\theta$, we come to the next condition on θ_L and $\delta\theta_L$:

$$2\theta_L + \delta\theta < \pi/2 \tag{2.6}$$

In practice, we will consider situations where $\sin(\theta_L) \leq \frac{1}{2}$.

2.3 Application to the SHS

Considering a plane wave arriving to the grating with an angle of Θ_L , corresponding to a Littrow wavenumber σ_L , the return angle will be $\Theta_L - \gamma$, with gamma supposed small. We insert these terms in the grating equation (2.1) and get:

$$\begin{aligned}
d(\sin(\Theta_L) + \sin(\Theta_L - \gamma)) &= \frac{m}{\sigma} \\
\text{with Taylor approximation for the sinus and } \cos(\gamma) &\text{ approximate to 1:} \\
2\sin(\Theta_L) - \gamma\cos(\Theta_L) &= \frac{m}{\sigma} \\
= \frac{\sigma_L}{\sigma} 2\sin(\Theta_L) & \\
\gamma\cos(\Theta_L) &= 2\frac{(\sigma - \sigma_L)}{\sigma} \sin(\Theta_L) \\
\gamma &= 2\frac{(\sigma - \sigma_L)}{\sigma} \tan(\Theta_L)
\end{aligned} \tag{2.7}$$

We can now replace in the period found for the Michelson Interferometer's fringes the value of α by the calculated value of γ :

$$\Delta x = \frac{\pi}{\pi\sigma \sin(4\frac{(\sigma - \sigma_L)}{\sigma} \tan(\Theta_L))} \tag{2.8}$$

We keep in mind that the angle is small compared to Θ_L . The sinus is equal to its argument:

$$\Delta x = \frac{1}{4(\sigma - \sigma_L) \tan(\Theta_L)} \tag{2.9}$$

The pattern on the screen will be:

$$I_r(x) = 1 + \cos\left(\frac{2\pi x}{\Delta x}\right) \quad (2.10)$$

In the expression corresponding to the Δx , i.e. equation (2.9) we see that the wave number difference appears at the denominator of the expression. Hence, the smallest the difference in wavelength will be, compared to the Littrow wavelength, the largest will be the fringe spacing. The limitation for the wave number difference will be the size of the fringe figure, that must not exceed the width W of the beam:

$$\Delta x < 2W \text{ i.e. } (\sigma - \sigma_L) > \frac{1}{8W \tan(\Theta_L)} \quad (2.11)$$

The resolving power of the system is given by the value $\frac{\lambda_L}{\Delta\lambda_{min}}$. Our expression was calculated for the wavelength and not for the wave number. Let's calculate the relation between the wavelength difference and the wave number difference. For small differences, we have in first approximation

$\frac{\Delta\sigma}{\Delta\lambda} = \frac{\partial\sigma}{\partial\lambda} = \frac{-1}{\lambda^2}$. We get after some calculation the following relation:

$$\frac{\partial\lambda}{\lambda} = -\frac{\partial k}{k}. \quad (2.12)$$

If we take the absolute value of the expression, the resolving power is of the same form in terms of wavelengths and wave numbers. For the following discussion, this results will be important to notice.

By considering positive deviations from the central wavelength (we want to have positive signs), we suppress the sign minus and get for λ close to λ_0 :

$$\Delta\lambda > \lambda_0^2 \frac{1}{8W \tan(\Theta_L)} \quad (2.13)$$

Dividing λ_0 by $\Delta\lambda$, we obtain the resolving power of the SHS:

$$\text{RESOLVING POWER} = \frac{4W \tan(\Theta_L)}{\lambda_0} = \frac{4W \tan(\Theta_L)}{2d \sin(\Theta_L)} \quad (2.14)$$

Let's assume that the grating consists in N grooves, we have $W = Nd \cos(\Theta_L)$ (The beam width is the projection of the grating length on the wave front). Simplifying the sines, cosines and tangent, we get the result that the resolving power is equal to $4N$. This result is independent from the Littrow wavelength. Hence, whatever the wavelength domain, the relative resolution is always constant for a given grating.

Taking the case of a grating of 2.5 cm width, with grooves of $1\mu m$, we get a resolving power of 100000. For a Littrow wavelength of 500 nm, the minimum $\Delta\lambda$ would be 0.0005 nm. With a radial velocity of about 50 m/s for a sun-like star surrounded by a hot Jupiter(at the distance of Venus,

for example), the ratio β would be 1.66×10^{-7} . The minimum resolving power for such a detection of Doppler shift would be 6×10^6 , which is about 100 times larger than the resolving power of a SHS as we consider it in the discussion. The only case where it seems possible to detect something like this would be a close binary system with a sun like star and a brown dwarf orbiting at a sufficiently close distance (0.01 AU) of the principal star. Therefore, it doesn't seem to be a good application of the SHS, at least if we consider the possibility to mount it on a CUBE SAT. However, if we consider higher speeds, such as speeds in galaxies, it would be possible to deduce rotation speeds of galactic disks and thus, estimate the dark matter quantities in galaxies, by estimating, for example, the deviation of Lyman- α ray.

The last limitation to take into account is the spectral band. Since we have a minimal wavelength difference, we can suppose that the wavelength domain is discretized. Thus, we will consider the maximum deviation from the central wavelength to be $N\Delta\lambda$. For a wavelength difference of $N\Delta\lambda$, the number of peaks is N. If we have M pixels, N must be smaller or equal to $M/2$. The bandwidth is twice the wavelength.

For the minimal wavelength difference, we had:

$$2W = \Delta x = \frac{\lambda_0^2}{\Delta\lambda \tan(\theta_L)} \quad (2.15)$$

For $\Delta\lambda = BANDWIDTH$, we get $\Delta x = \frac{2W}{N}$ and:

$$BANDWIDTH = \lambda_0^2 \frac{M}{4W \tan(\Theta_L)} \quad (2.16)$$

Coming back to our example and assuming a detector size of 1024 pixels, we get a bandwidth of 5.12 nm (with a Littrow wavelength of 500nm and a grating width of 25 mm). We see from the result, that even for a deviation of the wavelength close to the maximum deviation, the approximation of small angles holds, because the deviation is small, with regard to the Littrow wavelength.

As it is shown on the expression of the fringe pattern, we can see a major difference between the Michelson Spectrometer and the SHS. While the fringe pattern period is simply given by the absolute wavenumber of the incident wave for the Michelson interferometer, for the SHS, the fringe pattern is given in terms of wavenumber deviations. It can be interpreted in such a way that the Michelson interferometer is a SHS with a zero Littrow wavenumber (infinite Littrow wavelength). The groove separation is also infinite, in the case of a Michelson interferometer. Therefore, we can take an arbitrary Littrow angle and obtain the fringe pattern described in the section 2.2.

2.4 Parameterisation

2.4.1 Simulation

The following graph shows the fringe spacing in function of wavelength deviation for a Littrow wavelength of 500 nm and for groove density of 800, 1000, 1200 and 1400 lines/mm. The groove density have been chosen to fit with what is currently easily reachable in terms of grating manufacturing. Some grating present even a larger groove density, but the manufacturing cost increase with the groove density. A limit needs therefor to be fixed. Smaller groove density would, on the other side be of no interest, since the resolving power would be highly reduced, and therefore, the advantage of the SHS would vanish.

For a better lisibility of the graph, wavelength differences smaller than 1/1000 of the Littrow wavelength were not considered (the curves would appear too close to each other for differences close to the finest resolution. In accordance with the predicted bandwidth, the maximum wavelength difference has been chosen to be 1/80 of the Littrow wavelength (approximately 1/100).

The fringe spacing expressed in function of the wavelength can be shown to be:

$$s = \frac{\lambda_L}{2\Delta\lambda} d \cos(\Theta_L) \quad (2.17)$$

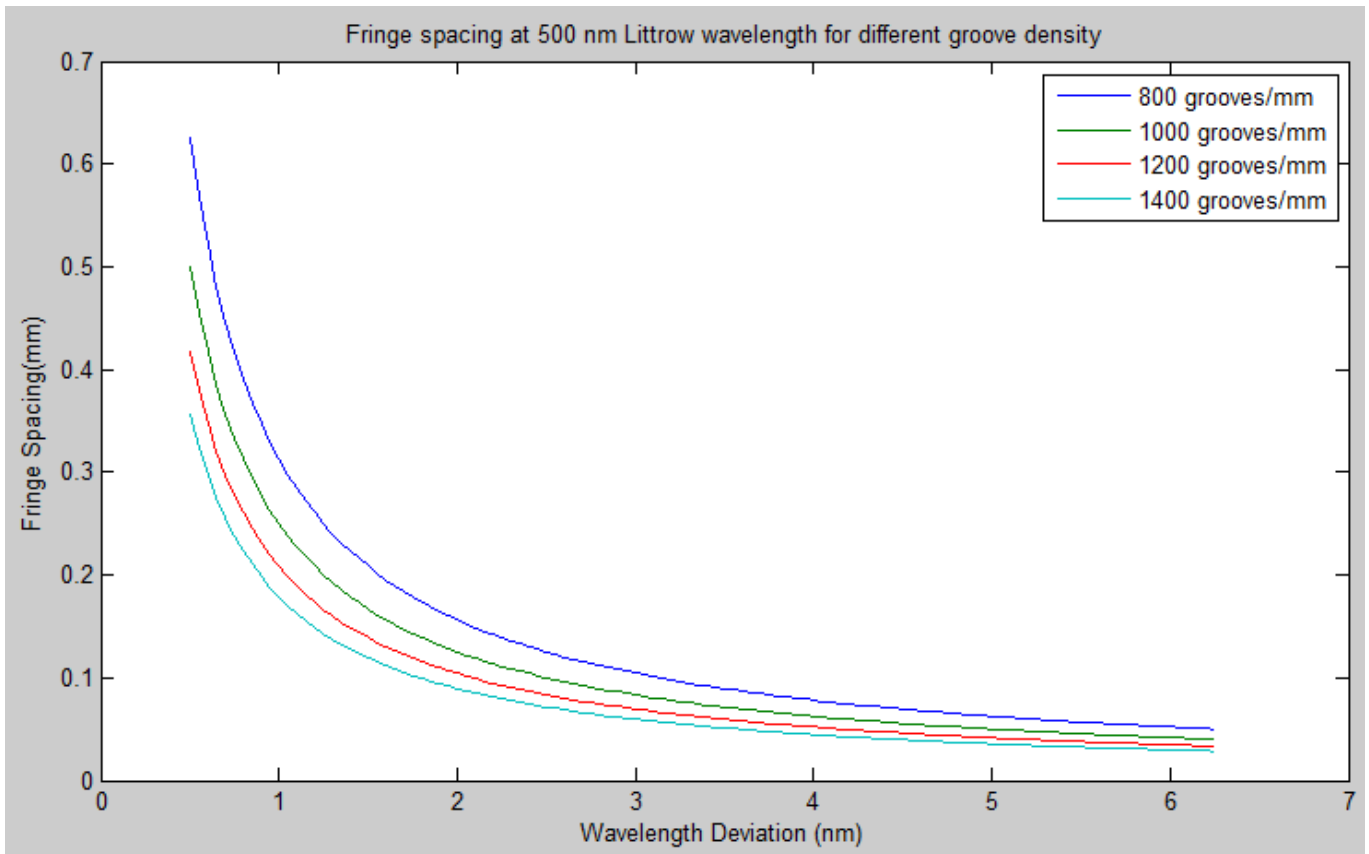


Figure 2.3: Fringe Spacing Simulation. In this example, a Littrow wavelength of 500 nm is assumed. We can see that the fringe spacing is inversely proportional to the groove density and to the wavelength difference. The dependence in groove spacing didn't appear explicitly in the expression involving wave numbers. Therefore, we can see the advantage to express the fringe spacing in terms of wavelengths. However, it was easier to find the expression of the resolving power starting from the expression in terms of wave numbers. The dependence in fringe spacing, in the expression in terms of wave numbers is hidden in the wave number difference variable. Another advantage to use wave numbers rather than wavelength, is that the Fourier transform gives of a space-depending function gives a wave number depending function. Hence, the spectrum that will be found will be expressed in terms of wave number. Finally, because of the proportionality, it will be easy to find the spectrum in terms of frequencies.

2.4.2 Discussion

We saw limitations in both resolving power (for stellar Doppler shift measurement, the resolving power is not high enough), and for bandwidth. Reminding the fact that For a resolution $\Delta\lambda$, the bandwidth is $M\Delta\lambda$, where M is the number of pixel, if we remind the fact that for grating with N

grooves the resolving power is $4N$, we have:

$$\Delta\lambda = \frac{\lambda_0}{4N} \quad (2.18)$$

$$BANDWIDTH = M/2 \frac{\lambda_0}{4N} \quad (2.19)$$

In the equations, λ_0 is simply the Littrow wavelength. We see that a lower number of grooves will allow a larger bandwidth. We also see that a larger detector allows a larger bandwidth.

Technically, it is also possible to raise the groove density up to approximately 2000 grooves/mm. This allows to have a better resolving power. The resolving power can also be refined by taking a wider grating. The design results in a compromise between bandwidth requirements and resolution requirements. The highest bandwidth achievable for a given detector size will be achieved for

$$N = M/2, \text{ with } N, \text{ the number of grooves and } M, \text{ the number of pixels.}$$

Even if 1024 pixels per detector row is a common value, it is reasonable to imagine a detector size of 4096 pixels/row. If we take $N = M/2$, the bandwidth achievable is equal to the Littrow wavelength. In such conditions, small angles approximations wouldn't hold any more. Limiting the bandwidth to one tenth of the Littrow wavelength seems a reasonable compromise.

Chapter 3

Comparison with other Spectrometers

3.1 Fabry-Perot Interferometer

The Fabry-Perot interferometer is a very simple device. It consists in two thin semi-reflecting blades and a cavity with a refraction index different from the surrounding medium (air for example). In practice, it will consist in a thick plate of glass with a thickness t (in this case, we speak about a Fabry-Perot etalon). For a light beam with incident angle i , we will have inside the plate a refraction angle θ . the figure on the screen will be given by concentric circles (also known as Newton rings) where the phase difference between two maxima will be:

$$\Delta\Phi = 4\pi knd \cos \theta \quad (3.1)$$

In this discussion, k is $1/\lambda$, d is the distance between the two reflective plates, so that the optical path difference is $OPD = 2d \cos \theta$.

The total transmittance can be shown to be:

$$\tau_{FP} = \frac{1}{1 + \frac{4R}{(1-R)^2} \sin^2 \frac{\Delta\Phi}{2}} \quad (3.2)$$

where R is the reflectance of the plates. The intensity on the screen becomes:

$$I_{FP} = I_0 \frac{1}{1 + \frac{4R}{(1-R)^2} \sin^2 \frac{\Delta\Phi}{2}} \quad (3.3)$$

with I_0 , the incident intensity. For an incident angle θ equal to 0, the intensity is maximum for a distance between the two plates that is multiple of $\lambda/2$, and the first peak occurs at a distance δ equal to $\lambda/4$, with a distance of $\lambda/2$ between two consecutive peaks.

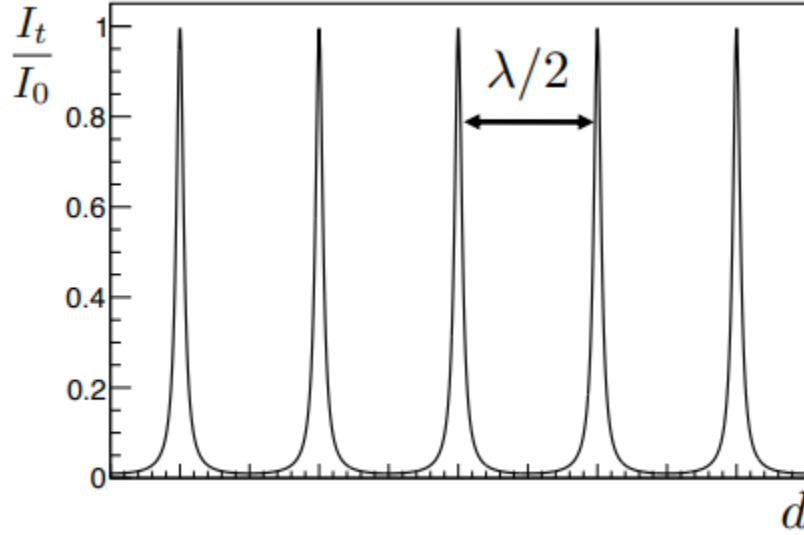


Figure 3.1: Fabry-Perrot fringe pattern

Only some wavelengths can be transmitted (i.e. $\lambda = \frac{2dm}{m^2+1}$, with d the distance between the plates and m an integer). That means that λ_m and λ_{m+1} are separated by a difference of $\delta\lambda = \frac{d}{m^2+1}$. The two consecutive wavelength can be distinguished on the fringe pattern, provided their separation is large enough:

$$\frac{\delta\lambda}{\Delta\lambda} \geq \frac{R^{1/2}}{1+R} = F \quad (3.4)$$

F is the finesse of the interferometer and R is the reflectance of the two plates. Finally, one can show for a low reflectance, that the fringe pattern for the Fabry-Perrot Interferometer becomes similar to a Fourier Transform interferogram:

$$I_{FP} \approx \left(1 - \frac{4R}{(1-R)^2} \sin^2(2\pi kOPD)\right) \quad (3.5)$$

Reminding the relation $\cos 2\alpha = 1 - 2 \times \sin^2(\alpha)$, we come with an expression of the type:

$$I_{FP} = A + B \cos(4\pi kOPD) \quad (3.6)$$

with A and B , some constants. The modulated expression corresponds to the modulated part of a Fourier Transform interferogram. However, even if the interferometer behaves like a Fourier Transform interferometer, to collect the full spectrum, moving plates are required because of the fact that the distance between the plates must be an entire multiple of the wavelength to collect the light. This requirement could in some case justify a Spatial Heterodyne Spectrometer, rather than a Fabry Perot Interferometer.

3.2 Michelson interferometer

As described earlier in this report, the Michelson interferometer is also a Fourier transform interferometer, meaning that the input spectrum is obtained by A Fourier Transform of the detected signal, which is a combination of sinusoids. However, to cover the bandwidth, for the Michelson interferometer, the different fringe patterns are obtained by tilting the mirrors, which requires moving parts for the system.

As mentioned in the introduction, moving parts must be avoided in space applications when possible. The SHS has the advantage to allow a construction of different fringe patterns without turning the mirrors. It is also possible to design a monolithic spectrometer, meaning that once built and calibrated, no additional calibration must be done during the mission, except perhaps some thermal measurements.

3.3 Scale grating

A first grating scattering the light with high dispersion order is placed in front of a second one, with an optical axis perpendicular to the first, so that the light is transmitted through a point and not a slit. The combination of the two gratings allows a very high resolution, independently of the wavelength, however because the high dispersion of the light, the intensity becomes very low. Such a spectrometer can only be used if the incoming flux is high enough. For sources that are too small or not bright enough, it won't be adapted.

Chapter 4

Space Applications

To fix the parameters, we must know characteristic of studied physical processes (typical bandwidth, typical precision on the wave number measure). From these parameters, we will be able to fix the Littrow angle (from the minimal wavelength), and the required resolving power. The resolving power will give us the number of grooves required for the measurements. Finally, the bandwidth will give conditions on the number of pixels in the detector.

4.1 Chemical Sounding of the Atmosphere

For many applications, the only way to get global estimations of atmospheric concentrations of chemicals, is to use space-based application. A way to determine the concentration of different chemicals is to use near or mid-infrared spectroscopy. A molecule excited by a source of light will absorb a quantity of energy and will re-emit it in a specific wavelength. The observation can be passive (the molecule will be illuminated by the sun), or active (in this case, it is frequent to excite the molecule by laser. The backscatter of the light will be characterized by emission lines, recorded on a spectrum. These lines are often very narrow, and a high resolving power can be useful to determine a specific molecule. For mapping the different components of the atmosphere, one will prefer a large spectral band. Depending on the application, one will either privilege spectral resolution or spectral band.

4.1.1 Limb Sounding of the Atmosphere

Limb sounding of the atmosphere consists in an observation of limb-scattered sunlight. Typically, it is a passive spectroscopy application. The light source is the sun and there is no need of built in light source. The limb sounding can study narrow and large spectral bands. Large spectral bands

will be used for mapping the constituents of the atmosphere, while narrow bands will be used for abundance study of one known constituent.

An existing application, named SHOW (spatial heterodyne observation of water) is already operational. The observed bandwidth is 1363-1366 nm, with a spectral resolution of 0.03 nm. The application is based on an airplane, but it is also possible, because of the compactness of the SHS to plan a satellite-based configuration of the application. For such an application, the resolving power will be privileged, rather than the spectral band. The light source is the sun and the spectrum must be calibrated to the Planck distribution at the temperature of the sun, corrected by the angle of sight of the sun (the lowest the sun is in the sky, the larger the peak wavelength will be). The other option for SHOW would have been to use a Fabry-Perrot spectrometer. However, in this case, to cover the required bandwidth, it is needed to have some moving parts, which is not the case for a SHS. Since the spacecraft is subject to vibrations during the launch phases, it is better suited for the mission to use a device without moving parts, which is the case of the SHS.

4.1.2 Pollutant survey of the Atmosphere using Raman Spectroscopy

The principle of Raman spectroscopy is to excite a dipolar molecule with a specific wavelength. For this purpose, a monochromatic light source is needed. Such a method is called an active spectroscopy technique.

When the molecule is in the excited state, it will release its excitation energy by emitting a photon. The final state of the molecule can have a different energy from the ground state (lower or higher). The wavelength will correspond to the energy difference between excited and desexcited states. The difficulty to apply Raman spectroscopy to atmospheric sounding will be the fact that the backscatter is often very weak in intensity. Furthermore, to study more than one component, it will be required to use both a tunable spectrometer and a tunable laser. In this study, we will focus our reflection on monolithic SHS. This kind of study can be taken into account if we only want to study one molecule (methane, CO₂, H₂O,...).

If the ground state is excited to the second excited state (or virtual state, depending on the input energy of the light source), and the final state is the ground state, we speak about Raman diffusion. If the final state is the first excited state, we speak about Stokes Raman scattering. Finally, if we excite the first excited state and return to the ground state, we speak about anti-Stokes Raman diffusion. The backscattered photon will have an energy corresponding to the difference between the energy levels.

For a given molecule, we will have three peaks located at three energy levels (anti-Stokes, excitation energy or pumping, and Stokes). To study the spectrum of a given molecule, the

bandwidth will be determined by the difference of energy between Stokes and anti-Stokes diffusion (typically, twice the difference between ground and first excitation states).

4.1.3 Water content study of the Martian Atmosphere

Similarly to the SHOW experiment, we will make limb sounding study, but this time not for the earth but for the red planet. Our source of light, considered for the Planck distribution (Black body, placed in front of the gas), will be the sun. We will also take into account the self emission perturbations due to the instrument temperatures.

Spectral Calibration of the SHS will be performed, assuming the presence, inside the instruments of two black bodes. this will allow to calculate the spectral responsivity of the instrument and the gain.

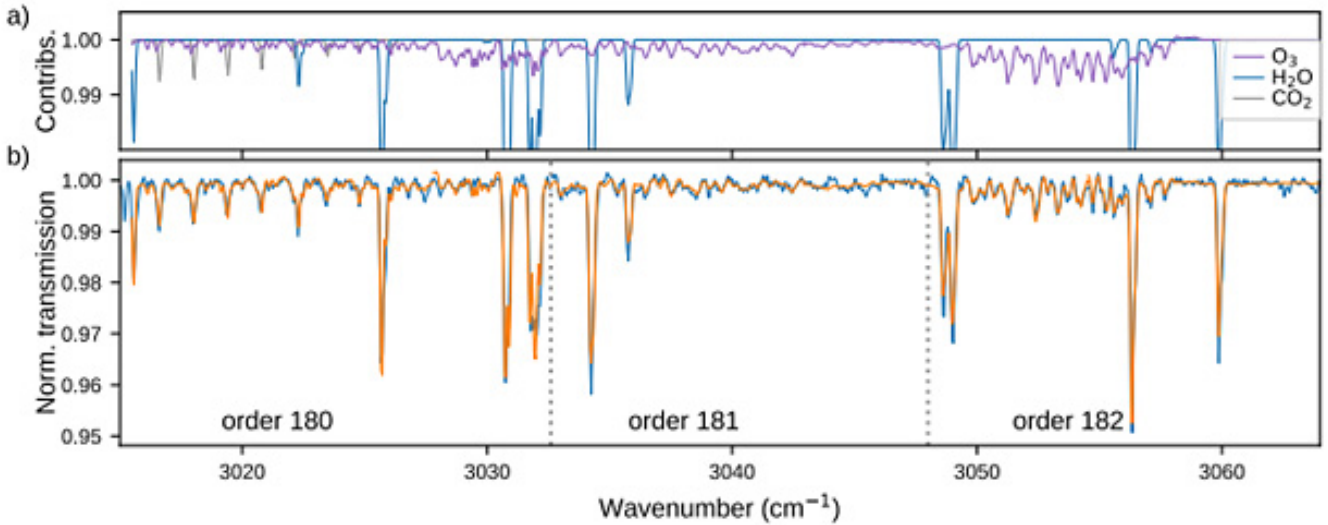


Figure 4.1: absorption spectrum of the martian atmosphere between 3020 and 3060 cm^{-1}

4.2 In Situ Sounding

4.2.1 Mineral study of Meteorites, Comets and other Objects with Raman Spectroscopy

If a material is excited with a light source of wavenumber k_{exc} , it can go back to it's initial energy state. In this case, we talk about Rayleigh scattering. However, it is possible to reach a virtual energy state E_v and then go back to another energy level than the initial one.

Starting from the ground level, corresponding to a wavenumber k_0 , and going to the virtual state of

wavenumber $k_0 + k_{exc}$, if the final state is the first excitation level, corresponding to a wavenumber k_1 , we have a Stokes Raman scattering

4.2.2 LIBS

Laser Induced Breakdown Spectroscopy is a technique of atomic emission spectroscopy. Like for the Raman spectroscopy, in the frame of molecules, it is an active method, meaning that an external light source is needed.

In this case, a high energy laser beam is pointed towards the studied sample, causing the vaporisation and atomisation of the components. The atoms are then excited and ionised in a high temperature plasma.

The excited atoms and ions return to their initial state, by emitting photons, which energy corresponds to the natural emission spectrum of the atom.

Such a method allows to measure the quantities of different elements in a solid sample.

4.3 Redshift measurements

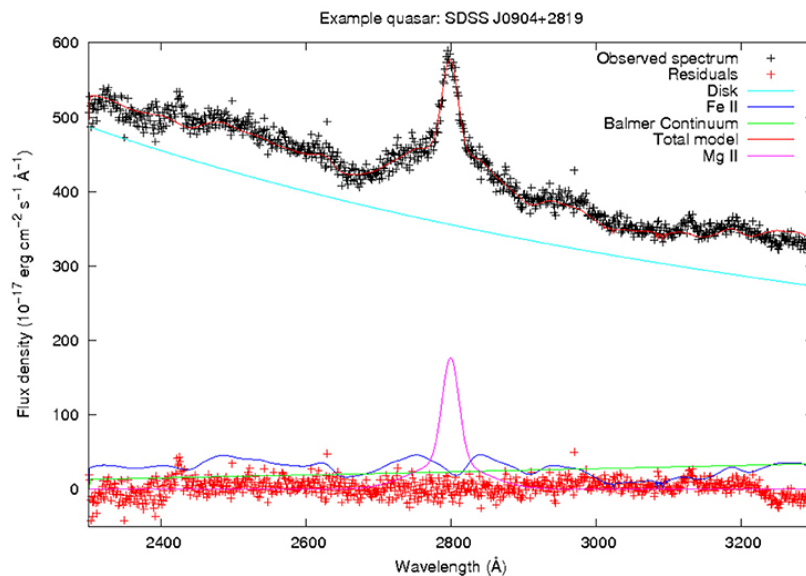


Figure 4.2: Final fit to the spectrum of quasar SDSS J090429.62+281932.7 (black crosses) showing all four spectral components and the total model. Residuals are the difference between the total model and the observed datapoints (source: Conor Wildy, Bozena Czerny, fpas)

Although the SHS is theoretically best suited for study of extended low intensity sources of light, it is possible (Alex G.KimaEric, V.Linderab, Jerry Edelsteinb, David Erskinec, GIVING COSMIC

REDSHIFT DRIFT A WHIRL, *Astroparticle Physics*, Vol 62, March 2015) to study redshifts of cosmological objects such as galactic disks or quasar accretion disks, provided, the instrument is coupled with a telescope. An example would be to mount a SHS spectrometer on the HST and to study the speeds in the accretion disk of a quasar.

In this thesis, the first application will be related to such a study. The Doppler redshift recorded on the spectrogram will be translated in a gaussian shaped emission line, instead of a narrow emission line. The MgII Line, in particular will be studied for our example. In this study, it will however not be possible to study in details factors such as self emission perturbations, because, we do not have enough thermal information on the source (the HST image of the quasar). However, we can optimize the dimensions of the device, which is also one of the purposes of the thesis.

The results of this simulation will be presented at first, because the approach is a simplified approach of the global approach, used for the limb sounding of Mars. However, if the program is correctly designed, it must be possible to have satisfying results, even if they are not perfectly realistic.

Chapter 5

Spectrum Recovery

We must distinguish in the output signal two parts: the first part is not modulated (it is simply the integral over the spectrum of the emittance), the second part is the signal modulated by a cosine function. The second part of the signal will be of interest in the discussion. We see that the output signal is a finite superposition of cosine functions over a finite portion of the space (the beam width). We can therefore conclude that the modulated part comes from a discrete cosine transform (or the real part of a discrete Fourier transform). To persuade of this assessment, we can simply remind that the Fourier transform of a periodic signal (or a signal defined on a finite domain) is a discrete signal. We can also remind that the Fourier transform of a discrete signal is a periodic (or finite domain signal). Because the image signal is both defined on a finite domain and discrete (we have a finite number of pixels), the signal that will be recovered will be also a discrete signal over a finite set of wave numbers. As a consequence of this discussion, we must also consider from the spectrum only a finite portion and discretize this signal. We will first analyze the behaviour of the signal for a delta-function at different positions, compared to the Littrow wave number. The signal on the detector will be simulated by considering imperfections of the detector as well as imperfection in wavelength dependent transmission. The signal on the detector will not be a cosine, since the signal will be modified by those factors. This will allow us to simulate the flat fielding process described by C.R. Englert and J.M. Harlander. Once this is done, we will consider two cases. The first case will be the case of a spectrum where the resolving power is determinant (typically, portion of a Raman spectrum), while the second case will be the case where the bandwidth is determinant (this could be the case if we want to measure the general transmittance of the atmosphere, for climatic models for example). In the second case, the general allure of the curve will be more determinant than the fast varying perturbations.

Knowing the order of magnitude for the natural incoming flux (given by the Planck distribution), if

we make assumptions on the temperature of the SHS, it will be possible to evaluate the signal to noise ratio, provided that we also consider the detector noise. The multiplicative detector noise can be assumed to be equal to the detector sensitivity. It's therefor removed by flat-field correction. But additive noise must also be taken into consideration and will result in a loss of resolution.

5.1 Detector Signal

5.1.1 Ideal Spectrometer

As seen above, for a given wave number deviation Δk , the signal at the output optics is given by:

$$I_r(x) = 1 + \cos(2\pi\nu_F x) = 1 + \cos(8\pi(k - k_L)\tan(\Theta_L)x) \quad (5.1)$$

Assuming a distribution at the entry optics $G(k)$, with $k = k_L - \Delta k$ (Δk is assumed to be positive and k_0 is the Littrow wave number, i.e. the maximum wave number), we have an integral expression for the signal at the exit optics:

$$I(x) = \int_0^\infty T(k)G(k)H(x)[1 + \cos(8\pi(k - k_L)\tan(\Theta_L)x)]dk \quad (5.2)$$

To select only the wave-numbers greater than the Littrow wave-numbers in our calculation, we will apply a band-pass filter allowing the light to pass for wave-numbers between k_{min} and k_L . The following filter is a good approximation of a real band pass filter, if we take α big enough:

$$Filter(k) = \frac{\arctan(\alpha(k - k_{min})) - \arctan(\alpha(k - k_L))}{\pi} \quad (5.3)$$

The signal has two components: the modulated part and the unmodulated part. $T(k_0 - \Delta k)$ is the transmission of the system. $H(x)$ is the As a first approximation, we can assume it to be constant ($\frac{1}{2}$), so that the maximum intensity corresponds to the entry optics intensity. The only part that is of interest to recover the input signal is the modulated part. We can note that the the modulated part of the signal is modulated by a cosine. The average value of the cosine over its domain is zero.

We can hence recover the modulated part of the signal at the output by subtracting the average value of the intensity at the output.

We must also note that the exit optics has a finite width. This will be translated on the recovered spectrum by a discretisation of the original signal (we consider that a signal defined on a limited domain corresponds to one period of a periodic signal), since the signal at the output is a superposition of cosine signals with each cosine having an entire multiple frequency of the signal frequency. We can show, that in absolute values, if the resolving power is given by $\frac{\lambda_i}{\Delta\lambda_{min}} = 4N$, it is also given by $\frac{k_L}{\Delta k_{min}}$. This will give us the minimal frequency of the signal at the exit optics.

We must also notice that the fringe density, $4\Delta k \tan(\theta_L)$ directly proportional to the wave number deviation, and that because of θ_L being constant, the Real part of the Fourier transform of the modulated part of the expression will give exactly the input spectrum, if we divide the x-coordinates in the recovered spectrum by $4\tan(\theta_L)$:

$$I_{RECOVERED}(\Delta k) = IFT(I(x)) \text{ at } (4\tan(\theta_L)\Delta k) \quad (5.4)$$

5.1.2 Ideal Image of a Delta Function Spectrum

Assuming that $I(k)$ is zero everywhere, except for a k_1 value, the image will be given by

$$I_r(x) = 1 + \cos\left(\frac{2\pi x}{\Delta x}\right) = 1 + \cos(8\pi(k_0 - k_1)\tan(\Theta_L)x) \quad (5.5)$$

With $\cos(8\pi(k_0 - k_1)\tan(\Theta_L)x)$, the modulate part, taking the inverse cosine transform (i.e. the real part of the inverse Fourier transform), we can guess what the recovered spectrum will look like. The fringe frequency is $4(k_0 - k_1)\tan(\theta_L)$. After Fourier transform of the interferogram, we will get the input spectrum, if we divide the x-axis by $\tan(\theta_L)$ and translate the axes by k_0 to the right. Taking in consideration the fact that the beam width is finite (between $-W/2$ and $W/2$), the signal at the detector is the product of the signal for an infinite detector by a door function (that have a sinc image by Fourier transform). Taking into account the fact that a Fourier transform of a product of functions is the convolution product of the Fourier transforms of the functions, the recovered spectrum of a delta-like spectrum will be a sinc-like spectrum.

In the following example, we suppose to have a Littrow wavelength of 500 nm. The spectrum is supposed to be zero everywhere, except for 19961/cm. The input wave numbers are defined between 19922/cm and 20000/cm. With a Littrow angle defined as being the arcsinus of 0.6, and a length of 24 mm, the number of grooves is 72000. We get a spectral resolution (one ray on the detector) of 0.173611/cm.

The detector is supposed to be of 900 pixels. That gives us 78/cm of spectral range. The scripts used to build the interferogram are presented in the annexes.

5.1.3 Ideal image for the Filter function

If the parameter alpha is sufficiently large (infinite limit), we recover a rect. function. The image by a fourier transform of a rect. function is a sinc function. Since the filter function is not exactly rectangle, the image will be a slightly modified sinc function

5.1.4 Recovery of the input spectrum

Taking the inverse Fourier Transform of the interferogram, one gets the spectrum in function of the fringe density. Since the fringe density is proportional to the wave number, a scaling of the x-axis will allow to recover the initial spectrum.

However, on the recovered spectrum, only one half of the image is data that we can use (since for N pixels, we can only retrieve $N/2$ different fringes, corresponding to wave numbers between δk and $N\delta k/2$, where $N\delta k/2$ equals the full bandwidth).

Since for negative deviations from the Littrow wave number and for positive deviations, the image is the same, we consider only the negative deviations for the input spectrum. The image recovered will correspond to the input spectrum, provided we take the right hand side of the recovered spectrum. On this recovered spectrum, one half will be non zero (corresponding to the input spectrum) the other half will be zero (since we put a filter).

The left hand side of the recovered spectrum corresponds to the mirror image of the recovered spectrum.

The process has been done for two cases of a delta-function to verify that the recovered image corresponds to the input spectrum. The interferogram is hard to read, because there are a lot of pixels considered on the image, as well as a large number of grooves (due to the fact that we try to have a high resolving power).

For the application, a Littrow wavenumber of 20000 cm^{-1} has been taken with a bandwidth of 62.5 cm^{-1} . For the first simulation, a peak has been modellized for a wavenumber of 19969 cm^{-1} and for the second, the peak is located at 19999 cm^{-1} .

The first simulation verifies the recovered spectrum, while the second simulation at very low wave number difference verifies the form of the interferogram.

For facility reasons, the sinus of the Littrow angle has been fixed, rather than the Littrow angle itself, for a value of 0.6. The beam width has been chosen to be 24 mm and the number of grooves has been taken to be 72000. The detector size has been taken to be 900. Therefore, the recovered resolution is a finite number of times the original resolution.

As seen On the following figures, the recovered spectrum and the original spectrum fit well together (the location of the peak for the recovered spectrum and the original spectrum are the same). The amplitude however is not exactly the same, because, the sensitivity has been taken into account. The recovered spectrum is simply a normalized spectrum, so that the integral of the spectrum over the whole bandwidth is one.

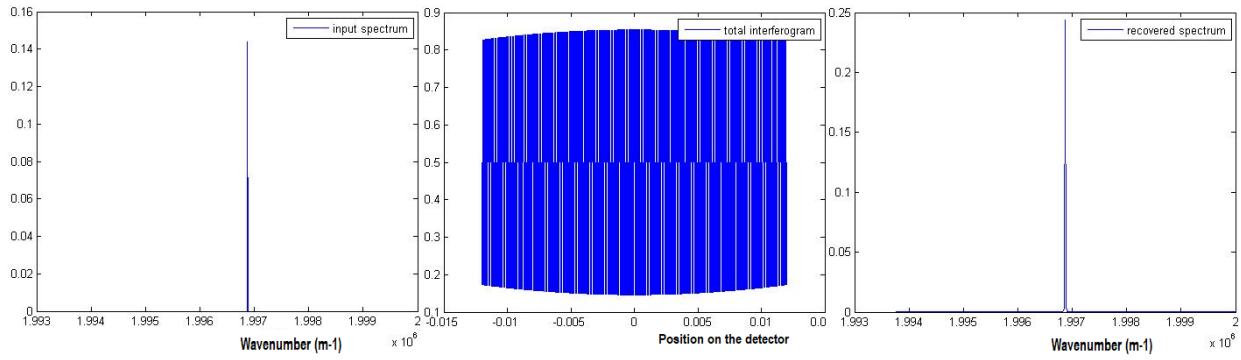


Figure 5.1: From left to right: original slightly modified "delta-shaped spectrum" centered at 19969 cm^{-1} , fringe pattern on the detector, recovered spectrum

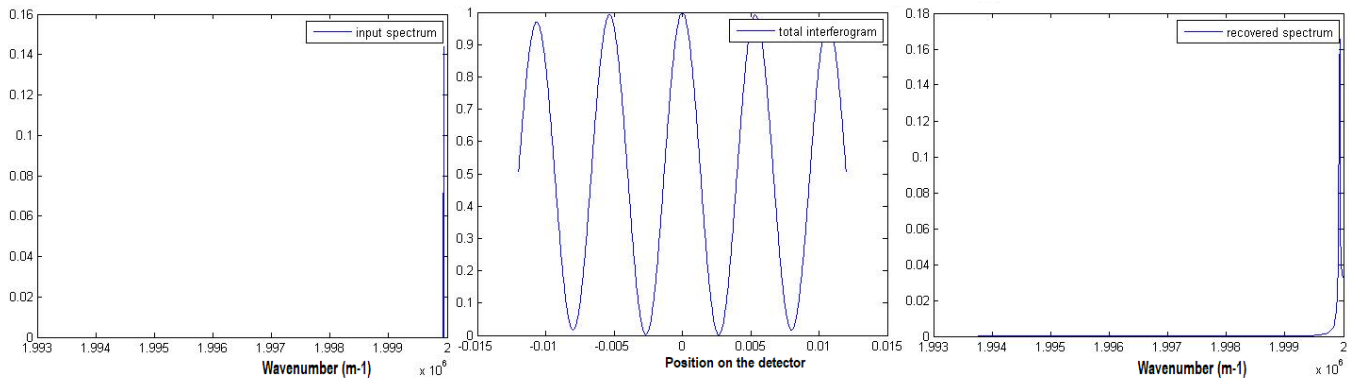


Figure 5.2: From left to right: original slightly modified "delta-shaped spectrum" centered at 19999 cm^{-1} , fringe pattern on the detector, recovered spectrum

Chapter 6

Signal processing for Applications

6.1 Device dimensions

In this section, rather than fitting a bandwidth to a given device, the dimensions of the instrument must be adapted to the requirement of the experience. In fact, for a real application, this is the way to process to design a mission.

The dimensions of the instrument were found, following an iterative process. A first estimation of the Littrow wavenumber and of the Bandwidth has been taken, then, the Littrow wavenumber has been taken slightly higher, and the bandwidth has been slightly larger, until the resulting dimensions allow a finite number of grooves as well as wavelength difference between two successive wavelength in the spectrum is a finite fraction of a finite number. Resulting of this, no irrational number must be measured to manufacture the instrument.

For a given application, we will have to fit bandwidth requirements. The size of the SHS will be determined by the mechanical constraints on the spacecraft (one unit cubesat). Therefore, the beam width will not be greater than 25 mm. We can also make choices for different detector arrays.

If the beam width is W , the detector size N_{pix} and the required band width $[k_{min}, k_{max}]$, let's consider the following triangle (top of the instrument, with hypotenuse being the grating):
From the grating equation, we know that the height of the triangle will be proportional to the sinus of the Littrow angle, while the base of the triangle will be proportional to the cosine of the Littrow angle:

$$\tan(\theta_L) = \frac{H}{W} \tag{6.1}$$

We also know that if the groove separation (which is measured on the hypotenuse is given by d , then the Littrow angle is given by $\sin(\theta_L) = \frac{\lambda}{2d}$

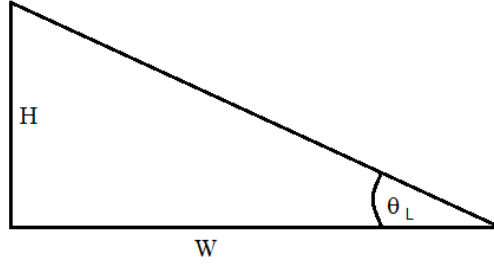


Figure 6.1: Triangle corresponding to the grating

If the number of grooves is N , we can calculate H easily:

$$H = N \frac{\lambda_L}{2} \quad (6.2)$$

We also have a simple relation between the tangent of the Littrow angle, the wavelength, the beam width and the number of grooves:

$$\tan(\theta_L) = \frac{n\lambda_L}{2W} \quad (6.3)$$

Given the required band width BW and given the resolving power of the grating, considering the Rayleigh criterion (to determine one ray on the detector we need at least two pixels, the resolution will give the smallest separation between two wave numbers. It is given by $\frac{k_L}{4N}$. With N_{pix} pixels, we can distinguish a maximum of $N_{pix}/2$ levels of wave numbers. We are therefore left with:

$$N_{grating} \leq \frac{N_{pix} k_L}{8BW} \quad (6.4)$$

Once the device is dimensioned to suit the bandwidth and resolution requirements of the context, we modelize the spectrum (or take a digitized spectrum, if it is available). For the two situations studied with matlab model, two approaches were performed.

For the model of the Doppler shift in the quasar disk, a naive approach has been performed (where we only consider the grating imperfections and the detector sensitivity, and neglect the thermal considerations). The advantage of this approach is to show easily the process of flat field correction and shift correction, since the interferogram will be modulated by the sensitivity functions of the two gratings only, and no additional term will perturb the interferogram, due to thermal emissivities.

Once the results and process of the quasar disk situation will be presented, we will consider the case of a martian atmosphere, exposed to the solar spectrum. We will study the absorption lines corresponding to water on a given bandwidth. For this situation, it is natural to introduce the instrument temperatures. As we will see, the naive approach and the more complex approach can be divided in two distinct steps in the global modelling of the instrument.

6.2 Doppler Shift in Quasar Disks

The input spectrum is modelized as a Gaussian function with the FWHM defined on figure (4.2), with some noise added. The spectrum is modelized for wavelengths between 270 and 290 nm. The total input Bandwidth is twice the coverage of the input spectrum (from Littrow wavelength minus the maximum difference to Littrow wavelength plus the maximum wavelength). The spectrum is then transformed into a wavenumber dependent spectrum:

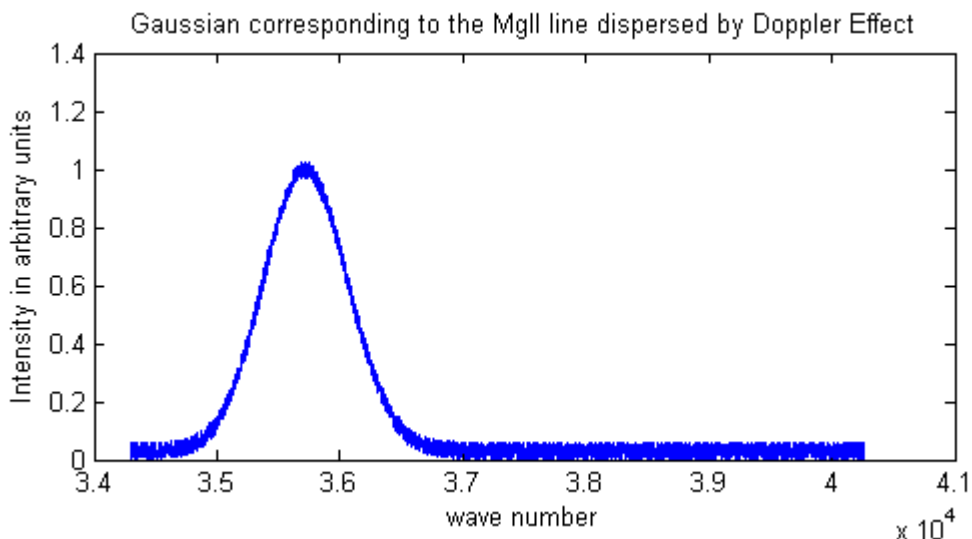


Figure 6.2: Reconstructed Gaussian corresponding to the MGII line in the quasar spectrum. The line is a gaussian because of the Doppler effect distribution

6.2.1 System Parameters

For this simulation we consider that the input spectrum is also the incident luminance studied. We neglect in this discussion the thermal considerations (for the atmospheric sounding, we will take them into account). However, we will suppose an error rate on the wavelength measurement. The

Parameters used for this simulation are:

$$\text{number of pixel } n_{pix} = 1024$$

$$\text{Littrow wavelength: } \lambda_L = 270nm$$

$$\text{error rate on wavelength measures} = 0.01$$

$$\text{beam width} = 2 \text{ cm}$$

$$\text{number of grooves}$$

$$\text{number of samples } N_S = 5$$

The number of grooves must be determined in such a way that the minimal bandwidth is covered with the pixel number of the detector. It should also facilitate the manufacture of the device (e.g.

by taking it of the form $5^M \times 2^N$. The minimal bandwidth is 20 nm. With the requirements, we can calculate the maximum resolving power, R_{max} , that can be taken to simulate the situation:

$$d\lambda_{min} = \frac{2BW_{min}}{n_{pix}} \quad (6.5)$$

with BW, the bandwidth in nm and n_{pix} , the number of pixel. Taking λ_l as Littrow wavelength, we have

$$R_{max} = \frac{n_{pix}\lambda_l}{2BW_{min}} \quad (6.6)$$

From the equation of the resolving power, we finally get:

$$N_{max} = R_{max}/4 = \frac{n_{pix}\lambda_l}{8BW_{min}} \quad (6.7)$$

With the previous parameters, we find that the maximum number of grooves is 3456. For the design, we take $N_G = 3200$. Finally, the spectrum is converted from wavelengths to wavenumbers. The spectrum is divided in NH sampling points equally distant between the two extremes of the bandwidth k_{min} and k_{max} .

6.2.2 General Processing Algorithm

The equation (5.2) describes the interferogram of the SHS in the case of ballanced arms (no considerations are taken of grating imperfections for the space-dependent correction factor $H(x)$). In practice, the grating also contributes for the space-dependent sensitivity.

We assume in this section $G(k)$ the spectral sensitivity and to be the same for both arms of the interferogram. However, the spatial sensitivity will be different for both arms, modellized by $t_a(x)$ and $t_b(x)$. These factors are stored in vectors of the same size than the detector.

The outcoming signal, if we consider $L(k)$ to be the product of the spectral sensitivity by the input spectrum will be given by:

$$I(x) = \int_{-\Delta k_{max}}^{+\Delta k_{max}} L(\Delta k)[t_a^2(x) + t_b^2(x) + 2t_a(x)t_b(x)\cos(8\pi\Delta k \tan(\Theta_L)x)]dk \quad (6.8)$$

with $\Delta k = (k - k_L)$ and Θ_L , the Littrow angle calculated from the parameters from previous section.

In the case of balanced arms, it would be easy to isolate the modulated term, however, in this case, it is not direct. This is done by applying a flat field correction. If we had thermal considerations, a

Dark current correction would have been done before.

After the Flat field correction, it might be possible that the center burst is not aligned with the *zero* - Δk . Therefore, a shift correction must also be performed.

As mentioned earlier, in this section, we consider also the deviation in wavelength measurements, that will also cause errors on position and angles:

6.2.3 Flat Field Correction

In equation (6.8), we can divide $I(x)$ in a modulated part I_M and an unmodulated part I_U . I_U can be found by blocking one arm then the other of the Interferometer. The intensities on the screen,

are I_a and I_b :

$$I_{a,b}(x) = \int_{-\Delta k_{max}}^{+\Delta k_{max}} L(\Delta k) [\tau_{a,b}^2(x)] dk \quad (6.9)$$

where $\tau_{a,b}$ is the spatial transmission function of respectively arm a or b. It is comprised between 0 and 1. The total intensity however is not greater than the intensity obtained by just a glass plate.

The maximum unmodulated intensity is hence less or equal to one half. The unmodulated part of the interferogram is:

$$I_U(x) = \frac{I_a(x) + I_b(x)}{4} = [t_a^2(x) + t_b^2(x)] C_1 \quad (6.10)$$

That leaves us with the following expression for $t_{a,b}$:

$$t_{a,b} = \frac{\tau_{a,b}}{2} \quad (6.11)$$

The flat field correction consists in two steps. The first step is subtraction of the unmodulated part, and the second step is the division by $\frac{2\sqrt{I_a \cdot I_b}}{\max(I_a + I_b)}$.

In this section, however, since we had the data for $t_{a,b}$, we simply divide the modulated part by $t_a t_b$.

6.2.4 Corrections due to Errors on Wavelength Measurements

The measure of the input spectrum is done on N sampling points λ_i . However, since the measure of

λ cannot be perfectly accurate, the real wavenumber corresponding to the i^{th} sampling point is $\lambda_i + \delta\lambda_i$. This error will also affect following variables, and thus affect the interferogram. However, since the goal of the simulation is to simulate with a given interferogram the spectral data, we will

suppose that only the measure of the Littrow wavelength is not accurate.

In this section, to minimize the effects of lack of accuracy on the measure of λ_L , we must suppose to have multiple sets of measure, that we will average. Starting from a Littrow wavelength that

differs from λ_L by $\delta > \lambda_L$, we have for the i^{th} set of measures:

$$k_{L,i} = \frac{1}{\lambda_L + \delta\lambda_{L,i}} \quad (6.12)$$

for the new Littrow wavenumber.

Also directly affected by the correction to the Littrow wavelength, we have the boundaries of the sampling domain in terms of wave numbers:

$$k_{max,i} = \frac{1}{\lambda_{L,i} - BW} \quad (6.13)$$

and

$$k_{min,i} = \frac{1}{\lambda_{L,i} + BW} \quad (6.14)$$

If the error rate of the Littrow wavelength is ϵ , so that $\lambda_{L,i} = (1 + \epsilon_i)\lambda_L$, the error rate for the tangent of the Littrow angle is the same (as shown on Figure 6.1): $\tan(\theta_{L,i}) = (1 + \epsilon_i) \tan(\theta_L)$.

6.2.5 Phase Shift Correction

There are, in theory two sources of phase errors. The first source is wavenumber dependent and will not be treated here, because it needs a monochromatic source to compare the spectrum. It is also quite tricky to put in place.

The second source is simply the shift of the center -burst for the interferogram, that might be shifted by a spatial shift of $+x_c$ from the zero path difference. The shift correction consists in correcting the shift:

$$I(x)_p = I(x) * \delta(c + x_c) \quad (6.15)$$

with $\delta(x + x_c)$, the dirac delta function centered at $-x_c$ and $*$ the convolution product. We can re-write the expression in terms of Fourier transforms (keeping in mind that the Fourier Transform of a Convolution product is the product of the Fourier Transforms):

$$I(x)_p = IFFT(FFT(I(x)).FFT(\delta(x + x_c))) \quad (6.16)$$

where the FT of $\delta(x - x_c)$ is $exp(i2\pi x_c.t)$. If we find the location of the center burst, we can multiply the FT of the intensity by the FT of the dirac delta function centered on $-x_c$ and then take the inverse Fourier transform of the product. Supposing the detector is divided in i sampling points separated by a distance dx , we find:

$$x_c = dx \left[\frac{\sum_i i |I(x_i)|}{\sum_i |I(x_i)|} - i_0 \right] \quad (6.17)$$

where i_0 is found by locating the sampling point corresponding to the maximum of the recorded interferogram. Because the interferogram is not continuous but discrete, even after centering the interferogram, the function may not be symmetric. The final step is to symmetrize the corrected interferogram.

6.3 Mars Atmospheric Water Lines

The spectrum described on Figure 4.1 is the mainly composed by a total transmitting band. On the unit transmission spectrum, we can distinguish the absorption lines corresponding to the water spectrum. The spectrum corresponds to the upper layer of the martian atmosphere and describes the transmission in direct incidence. To simulate limb sounding, we can suppose a thicker layer of atmosphere.

The lines are modelled as a square of a sinus defined on only one period. The function that represents the spectrum is thus no longer an analytical function. Furthermore, the sensitivity variations between the different positions on the detector adds some corrections that will cause the function to be non analytic. Modelling the atmosphere in this way will be a good way to estimate the behavior of the interferogram as well as the recovered spectrum.

If the atmosphere layer to consider had been only the one considered on Figure 4.1, the amplitude of the peaks, combined with their narrow width would have caused them to be confused with noise. In this section we tried to find the minimal layer to be able to rebuild the incident spectrum and came out with a layer twelve times thicker than the original one. With such a consideration we obtained following spectrum:

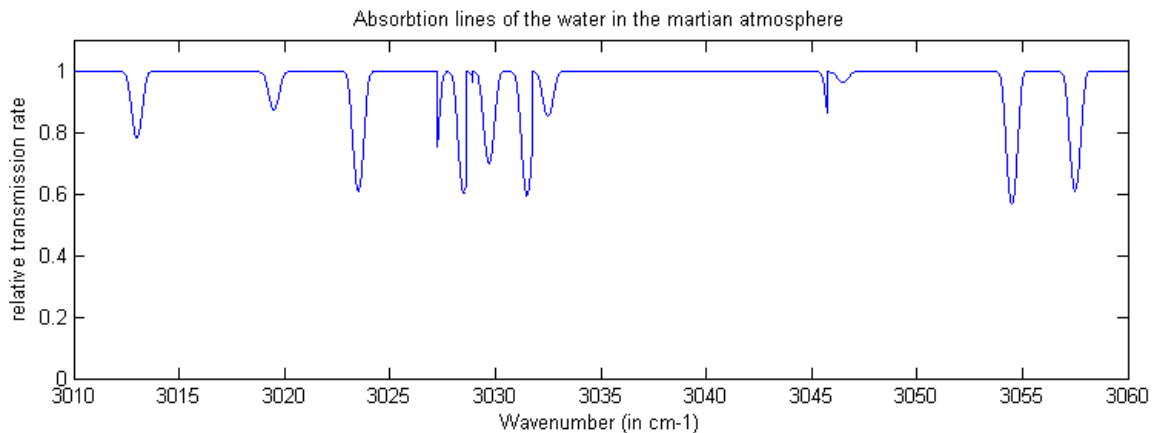


Figure 6.3: Input spectrum as modelled in matlab for the study of the martian atmospheric water absorption lines

6.3.1 System Parameters

First of all, we mention the fact that this section is meant to simulate thermal considerations on the system. We will first enumerate some thermal parameters as well as some physical constants:

$$\text{Speed of light: } c = 3 \times 10^8 [m/s]$$

$$\text{Planck constant: } h = 6.26 \times 10^{-34} [J.s]$$

Boltzmann's constant: $k_B = 1.38 \times 10^{-23}[J.K^{-1}]$

Solar solid angle: $\Omega_{sun} = 4 \times 10^{-5}[sr]$

Total system field of view : FOV=0.18[sr]

Temperature of the Sun: $T_{sun} = 5100[K]$

Entrance optics temperature: $T_{in} = 150[K]$

Exit optics temperature: $T_{out} = 120[K]$

Hot calibration black body: $T_H = 155[K]$

Cold calibration black body: $T_C = 145[K]$

The next parameters are associated to the spectrum and to the SHS itself. They are the same than for the case of the Doppler shifted MgII line in the Quasar accretion disk. Only the values are changed:

Littrow wavelength: $\lambda_L = 3240[nm]$

Band width: BW=81[nm]

Beam width: W=32[mm]

Number of grooves: $N_G=5120$

Minimal wavenumber: $k_{min} = 3011.1[cm^{-1}]$

Maximal wavenumber: $k_{max} = 3161.7[cm^{-1}]$

Littrow Angle: $\Theta_L = 0.2536rad$

6.3.2 General Processing Algorithm

For this simulation, we didn't take into account the error on the Littrow angle measure. However, we took into account the thermal considerations. We took as light source the sun, supposed to be a black body of homogeneous temperature with a solid angle of Ω_{sun} . The first step is to place the sample (extended atmosphere, because we are in the frame of Limb sounding) in front of the sun.

This is done by multiplying the spectrum by the Planck distribution of a black body of same temperature than the sun and multiplying the result by Ω_{sun} .

The second step is to consider the temperature at the entrance optics, by adding the Planck distribution corresponding to this temperature.

The light is then split by the beam splitter and goes to the gratings, once against supposed to have imperfections causing spatial transmittance to be affected. We treat separately both of the arms of the interferometer.

Finally, we consider the temperature of the detector, that will add a constant signal to the interferogram as well as to the signals obtained by blocking one arm or the other.

The next step is the Flat field correction, that is, if we did care correctly for the construction of the

signals I_a and I_b done in the same way than for the case of the Doppler shift in the spectral line of the Quasar.

Finally, the central burst is aligned with the two central pixels of the detector by the same method as mentioned previously for the Quasar.

The process to recover the input signal is described in the next section.

6.3.3 Thermal Considerations

This part, inspired by C. Perkins (Merrimark College, 2013) presents however a slightly different approach to the thermal considerations, especially due to the fact that in our case, the spatial sensitivity behaves randomly between 0.6 and 0.7, and not the spectral transmittance. This will lead to another form for the expression of the interferogram, that really takes into account the respective expression of the signal obtained for both arms separately of the interferogram. Notice also the slight modification in the approach of the flat field correction when comparing with the approach of Harlander and Englert.

The spectral radiance of the input is obtained by placing a sample of transmittance described in the Figure in front of a black body corresponding to the sun as seen from Mars. The units are $\frac{W}{m^2 sr.cm^{-1}}$. Multiplied by the solid angle of the Sun as seen from Mars, we obtain the input spectral emission. At the n^{th} sampling point of the spectrum k_n , we have:

$$L(k_n, T_{sun}) = \Omega_{sun} \tau(k_n) Planck(k_n, T_{sun}) \quad (6.18)$$

with $Planck(k_n, T_{sun})$, the Planck distribution at the sampling point of wavenumber k_n at the temperature of the Sun and τ , the total spectral transmittance, i.e. the product of transmittance of the atmosphere by the transmittance of the entrance optics. We suppose that the spectral efficiency of the gratings is the same for both sides, so that it can be included in the spectral transmittance of the entrance optics.

$$Planck(k, T) = 2hc^2 k^3 \frac{1}{exp\left[\frac{hck}{k_B T} - 1\right]} \quad (6.19)$$

The self emission term of the entrance optics is the Planck distribution of a black body at temperature T_{in} with a solid angle of 1sr. We get:

$$L'(k_n, T_{sun}) = L(k_n, T_{sun}) + Planck(k_n, T_{in}) \quad (6.20)$$

For respectively arm a and arm b, taking into account the spatial transmission, we get:

$$L''_{a,b}(k_n, x_m) = \eta_{a,b}(x_m) L'(k_n) \quad (6.21)$$

The interferogram becomes then, taking into account the fact that only one half of the separate contribution both arms contributes in the interferogram:

$$I(x_m) = \sum_{n=-N_h/2}^{n=N_H/2-1} \left[\frac{1}{2}(L_a'' + L_b'') + \frac{1}{2}\sqrt{L_a''L_b''}\cos(2\pi(k_L - k_n)4\tan(\theta_L)x_m) \right] dk \quad (6.22)$$

Finally, after the exit optics, with a detector spatial sensitivity η_d and an exit optics temperature of T_{out} , we get the expression of the interferogram measured on the detector:

$$I_d(x_m) = \eta_d(x_m) \left[I(x_m) + \Omega_{syst} \sum_n Planck(k_n, T_{out}) dk \right] \quad (6.23)$$

We can now perform the flat field correction and the phase shift correction in a similar way to the one used for the Doppler shifted spectral ray of MgII, previously.

6.3.4 Calibration of the Recovered Spectrum

Once the recovered spectrum is calculated, we must still calculate the gain and the detector responsivity, so that, for a given input spectrum, the amplitude of the recovered spectrum fits with the amplitude of the input spectrum. To perform this calibration, we must have reference responses of the system.

The simplest way to calibrate the recovered spectrum is to use as reference the Planck distribution of two black bodies of temperatures T_H and T_C . The recovered spectral radiance, for a given responsivity $r(k)$ and a given gain $g(k)$ is:

$$L_{rec}(k) = r(k)[L_{in}(k) + g(k)] \quad (6.24)$$

Thus, if we want to recover the input spectrum, we should make following operation that requires an estimation of $r(k)$ and $g(k)$:

$$L_{in}(k) = \frac{L_{rec}(k)}{r(k)} - g(k) \quad (6.25)$$

The temperatures T_H and T_C are chosen in such a way that T_H is slightly above and T_C slightly below the ambient temperature. Thus, between T_C and T_H , the difference of the recovered spectra is proportional to the input spectra corresponding to the reference black bodies, with a proportion factor of $r(k)$:

$$r(k) = \frac{L_{rec,H}(k) - L_{rec,C}(k)}{L_{in,H}(k) - L_{in,C}(k)} \quad (6.26)$$

that gives for the expression of the gain the result:

$$g(k) = \frac{L_{rec,C}(k)}{r(k)} - L_{in,C}(k) \quad (6.27)$$

6.3.5 Noise

Before starting with the study of the noise, we must introduce some additional parameters that are also involved for the noise:

$$\begin{aligned}
 &\text{pixel size: } A_{pix} = 4 \times 10^{-10} [m^2] \\
 &\text{integration time :} t_{int} = 1/500s \\
 &\text{Quantum efficiency: } Q_{eff} = 0.7 \\
 &\text{frame rate: } T=50[\text{frames/sec}] \\
 &\text{specific detectivity: } D^* = 10^{12} [Wm^{-1}Hz^{-1/2}] \\
 &\text{system aperture area: } A_{syst} = 9 \times 10^{-4} [m^2] \\
 &\text{noise power spectral density: } NPSD=10^{-7} [VHz^{-1/2}] \\
 &\text{Responsivity: } Res=100 [VW^{-1}] \\
 &\text{number of bits: } n_{bits} = 20 \\
 &\text{calibration error rate: } \epsilon_{cal} = 0.0001 \\
 &\text{bit error rate: } \epsilon_{bit} = 10^{-9}
 \end{aligned}$$

Following secondary parameters are then derived from the basic parameters:

Conversion factor from spectral radiance to number of electrons:

$$C_1 = \frac{(k_{max} - k_{min})A_{pix}\Omega_{sun}t_{int}}{hck_{rec}} \quad (6.28)$$

where k_{rec} is the spectrum in wave numbers sampled on the recovered domain.

Conversion factor from irradiance to number of electrons:

$$C_2 = \frac{A_{pix}\Omega_{sun}t_{int}}{hc(k_{rec})_{avg}} \quad (6.29)$$

and finally the conversion factor from noise in the spectral domain to noise in the space-domain:

$$C_3 = \sqrt{2/N_{rec}} \quad (6.30)$$

The method to build the noise signal has been inspired by the master thesis of C.Perkins (Merrimark College, 2013). A full description of the different noise sources can be found in her thesis.

The signal on the detector corresponds to a number of incident electrons reaching each pixel. This is also the case for the Noise, that is, for the main source of noise, i.e. the shot noise, assumed to follow a Gaussian distribution. Therefore, we can assume the standard deviation of each noise source to be proportional to the associated noise and the total standard deviation to be the square root of the sum of the individual contributions to the standard deviation.

Considering the fact that the signal is a number of electron, and taking the signal as measured on the detector (i.e. including the thermal considerations from above), the signal becomes, in terms of number of electrons $meas(x) = I(x)C_2$, so that the shot noise is simply $\sigma_{shot} = \left[\sqrt{S_{meas}(x)} \right]_{avg}$.

The next noise source is the calibration noise, caused by temperature changes in the calibration black bodies:

$$\sigma_{cal} = \epsilon_{cal}\sigma_{shot}^2 \quad (6.31)$$

Shot and calibration noises are both calculated for the interferogram domain. In the spectral domain, we have:

the detector and readout noise:

$$\sigma_{detec} = \left[\frac{2}{A_{syst}\Omega_{sun}D^*} \right]_{avg} \frac{\sqrt{A_{pix}TC_1}}{\left(\frac{\eta_a+\eta_b}{2}\right)_{avg}} \quad (6.32)$$

the electronic noise

$$\sigma_{el} = \frac{C_1(2W_{beam}NPSD\sqrt{T})_{avg}}{(A_{syst}\Omega_{sun}Res)\left(\frac{\eta_a+\eta_b}{2}\right)_{avg}} \quad (6.33)$$

the bit noise

$$\sigma_{bit} = \sqrt{\frac{\epsilon_{bit}}{n_{bit}} \sum_{q=0}^{n_{bit}-1} \left[\frac{2^q L_{max}}{2^{n_{bit}} - 1} \right]^2} \cdot C_{1,avg} \quad (6.34)$$

and the quantization noise, due to the rounding of measurement values to a certain precision:

$$\sigma_{quant} = \frac{L_{max}}{\sqrt{12}(2^{n_{bits}} - 1)} C_{1,avg} \quad (6.35)$$

with L_{max} , the maximum accepted radiance. The next step is to calculate the total standard deviation. Shot and calibration noises must be divided first by C_3 to be converted into x-noise.

Then summing the squares and taking the square root of this sum, we get the NESR (Noise equivalent spectral radiance) by dividing the result by C_1 :

$$NESR = \frac{1}{C_1} \sqrt{(\sigma_{shot}C_3)^2 + (\sigma_{cal}C_3)^2 + \sigma_{detec}^2 + \sigma_{el}^2 + \sigma_{bit}^2 + \sigma_{quant}^2} \quad (6.36)$$

The signal to noise ratio can then be calculated dividing the recovered signal by the NESR:

$$SNR = \frac{L_{rec}}{NESR} \quad (6.37)$$

6.4 Spectrum Recovery

Once all the treatment of the detector signal is done, we can recover the input signal by the mean of a Fourier Transform:

$$L_{rec} = \frac{1}{dk} |iFFTshift [iFFT(iFFTshift(I))] | \quad (6.38)$$

The operation iFFTshift aligns the center burst of the signal with the 0 input variable.

The recovered spectrum is still not the input spectrum. Between 1/4 and 3/4 of the recovered domain, we have the sum of $L_{recovered}(k)$ and $L_{recovered}(-k)$. Thus to find the input spectrum (or its approximation), we select the central half of the graph and keep only the left part of the graph. The next section will present the results (input spectrum, interferogram, recovered spectrum, recovered spectrum on restricted domain and comparison with the input spectrum on the same domain, and finally for the case of the study of the martian atmospheric water, the SNR graph).

6.5 Summary and Results

The general process to treat the interferogram is summarized in figure 6.4:

Incident lighth goes to the entrance optics O_1 with characteristic temperature T_{ent} . The light income that was L becomes now L'.

L' is split into L'_1 and L'_2 after being reflected by gratings g_1 and g_2 .

After recombination in exit optics O_2 , the detector D collects the interferogram $I(x)$. This interferogram is flat field corrected and shift corrected (in our case only at the level of the center burst location). If there are many samples, the interferograms are then averaged. An inverse Fourier Transform gives the recovered spectrum, that should ideally fit to the input spectrum.

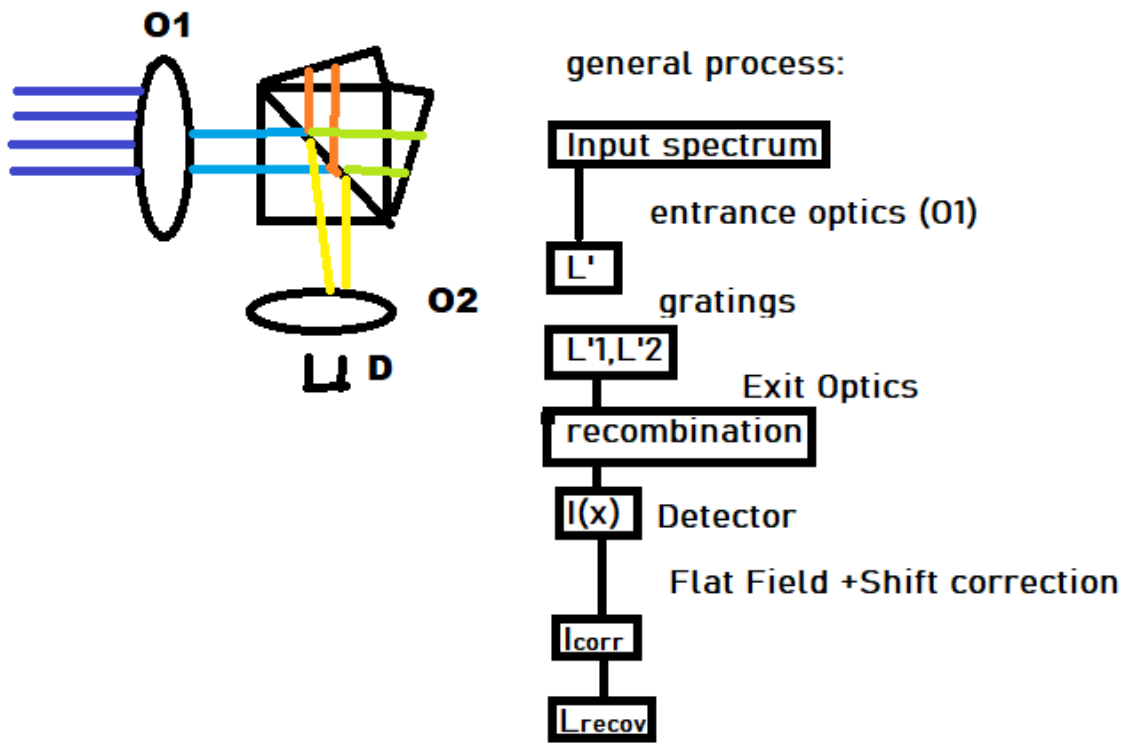


Figure 6.4: general process to treat SHS Interferogram

6.5.1 Doppler Shift in Quasar Disks

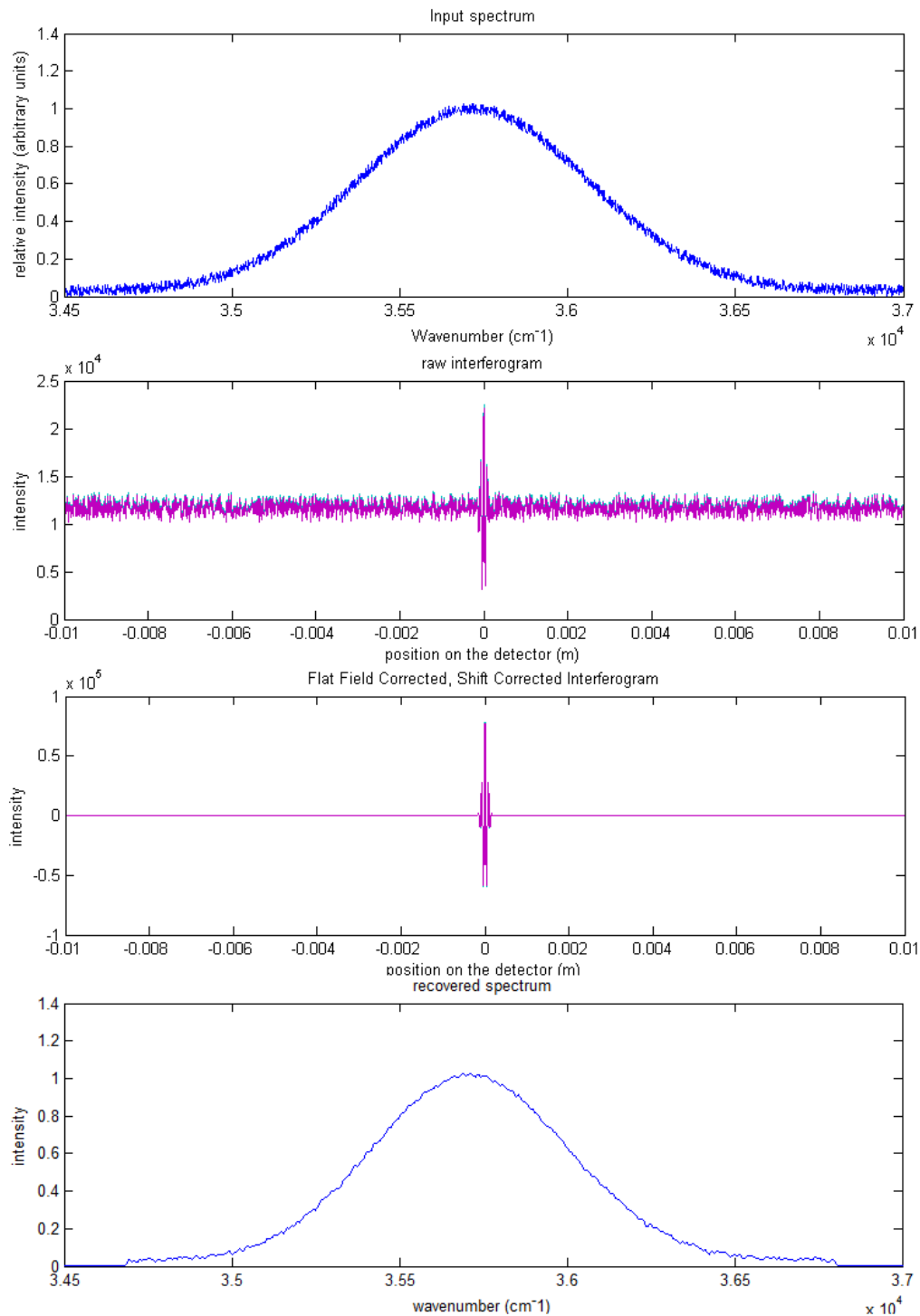


Figure 6.5: From top to bottom: The input spectrum corresponding to the spread MgII line, the raw interferogram, the corrected interferogram, the recovered spectrum

The second and the third figures of Figure (6.5) are respectively the raw and the flat field and shift centered interferograms. The raw interferogram looks quite noisy because of the variability of the

detector sensitivity and because of the grating imperfections. However, with a higher number of samples (we have only five of them, it would tend to be also quite flat, and, in this case, the unmodulated part that is used for the flat field correction would have been a constant. The last figure, the recovered spectrum, seems to fit quite well to the input spectrum, however, to be sure that it's the case, we should treat a case where the characteristic functions are narrow lines. This is the case of Raman spectra, but also of spectral absorption lines, which has been done in the next paragraph.

6.5.2 Mars Atmospheric Water Lines

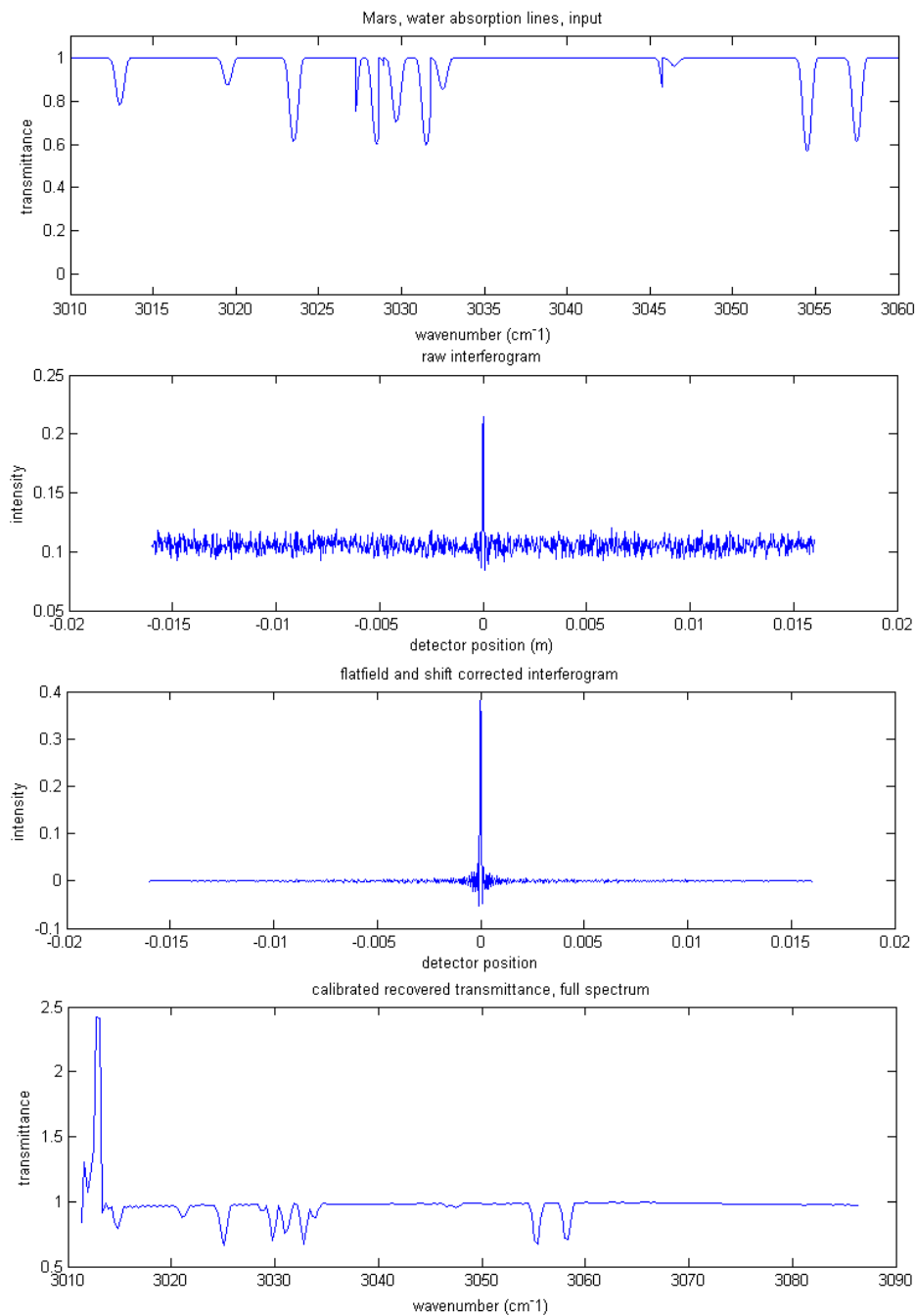


Figure 6.6: From top to bottom: The input spectrum corresponding to the H₂O lines in martian atmosphere, the raw interferogram, the corrected interferogram, the recovered spectrum

We see for the recovered spectrum with non restricted domain at the left edge, a peak. The Fourier series, just like splines or other series are not able to reproduce entirely a spectrum, unless the number of basic function is infinite. If we would add more and more basic functions to the serie, we would have had an even higher peak at the edge of the domain, but this peak would have been

much narrower.

However, we can already see that for the spectral lines (negative peaks in the constant transmittance), the pattern looks quite similar to the original pattern. The next two figures will be defined on the same restricted domain, so that a more accurate comparison can be done.

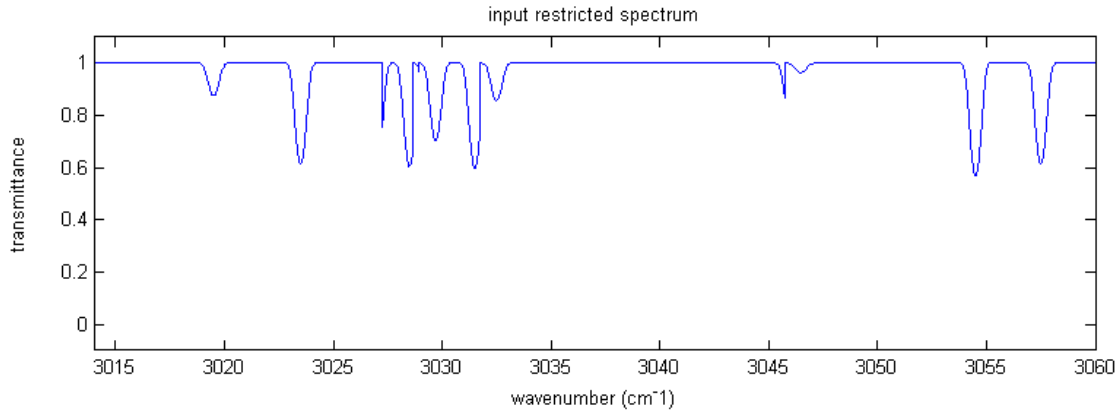


Figure 6.7: restriction to the domain of input spectrum

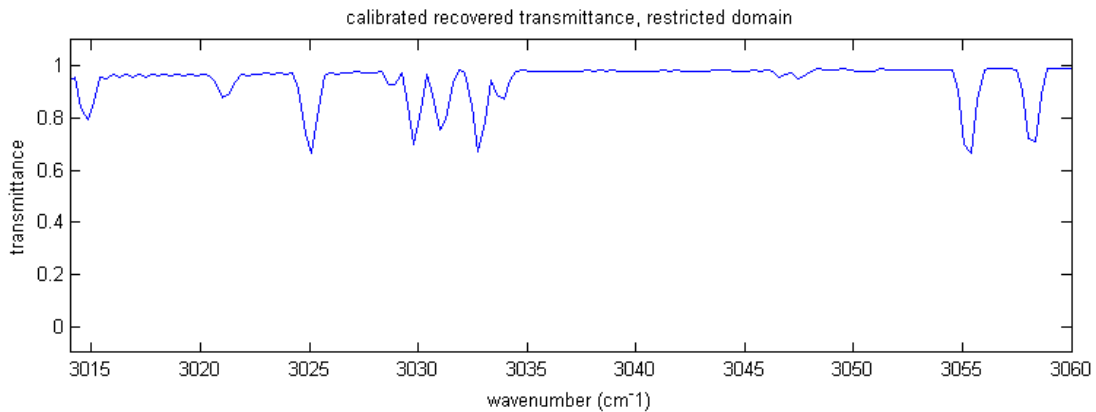


Figure 6.8: restriction to the domain of calibrated recovered spectrum

As one can see, when one deviates more from the Littrow wave number, the location of the peak ceases to be conform to the original spectrum. This phenomenon is called phase distortion. One can correct this effect, however, to perform this, it would involve some tricky codes in matlab, and it was asked to keep it quite simple. A description of the process can be read in [Jilin Liu et al. Analysis and correction of distortions in spatial heterodyne spectrometer system. Applied Optics, 58(9):2190–2197, 2019.]. The results, however, suggest the feasibility, with some more time of such a correction.

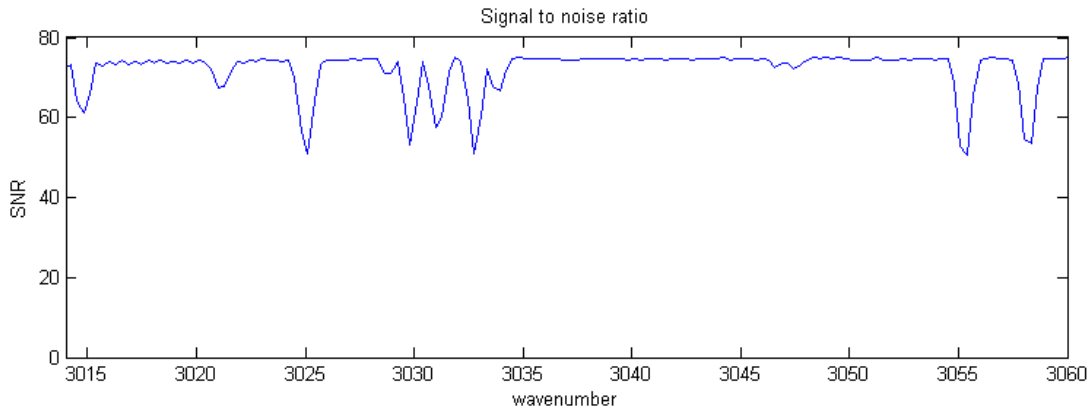


Figure 6.9: Signal to Noise Ratio for the study of the Martian atmospheric water

A comparison between Figure (6.9) and Figure (6.8) shows that the SNR is quite proportional to the signal, meaning that for the spectral width, the expected noise is relatively proportional. The main contribution to the noise is the shot noise. Since this noise is proportional to the square root of the integration time, whereas the signal is proportional to the integration time, increasing the integration time would decrease the noise by a factor proportional to the inverse square root of the increasing factor of the integration time.

However, in the simulation, since the saturation level of the detector has been fixed at 1.2 times the maximum recorded spectrum, the SNR would be also bounded by 1.2 times the SNR calculated here. We have, however a signal that is fifty times as strong as the noise, which seems reasonable.

Conclusions

The feasibility of a SHS, with restricted place, in order to include it in a CubeSat seems to be demonstrated, which was one of the goals of the work done.

It has also been shown that for smooth curves as well as for curves composed by series of peaks, the provided the number of pixel is large enough, the typical gratings can produce a sufficiently high resolution to recover correctly the input signal.

However, to reproduce correctly the input signal, one should be able to modelize the phase distortions, and thus the wavenumber distortion that have been detected in the case of the study of the martian atmospheric water lines.

Such a work could be performed in a future work.

It can also be mentioned that the codes had to be done alone and not within a team. Some more detailed study would have been feasible within the previously allocated time, provided some help would have been available for the coding of the calculations.

One can also notice, that, in the frame of the pandemics, tests based on Raman spectroscopy focused on the characteristic spectrum of the SARS-COV2 are to be developed in Asia. Such a test could also be, even if it's not a space application, an interesting application to miniature SHS.

Matlab Codes

Note: all the following codes must be grouped into specific folders (simple model, Doppler Shift in Quasar Disks, Mars Atmospheric Water Lines), so that the required codes to run the section are placed together.

Simple Model

simplemodel.m

```
1  clc
2  %% This script simulates a response of the detector to a monochromatic
3  %% light source for an ideal one dimensional SHS.
4  %% (transmissions are supposed to be constant, pixel sensitivity
5  %% is supposed to be one everywhere, arms are supposed to be perfectly
6  %% ballanced)
7  %% For the spectrum recovery, we will select only the negative wave number
8  %% differences (since we defined the littrow wavelength to be the maximum
9  %% wavelength)
10 %% Parameters
11 % length units are meters, whatever the measurement (x-position on the
12 % detector, beam width, grating distances, wavelengths. The conversion in
13 % other units will be done for the plots.
14 thetaL=asind(0.6);
15 sigmaL=1/(5*10^(-7));
16 npix=900;
17 L=0.024;
18 dgrating=1/(2*sigmaL*0.6);
19 disp('Littrow wave number is')
20 disp(sigmaL)
21 N=0.03/dgrating;
22 specrange=npix/(0.024*8*tand(thetaL));
```

```

23 disp('Spectral range is')
24 disp(specrange)
25 disp('N=');
26 disp(N);
27 dkmin=1/(4*L*tand(thetaL));
28 disp('best resolution is');
29 disp(dkmin);
30 bandwidth=npix*dkmin/2; %Rayleigh criteria
31 disp('Bandwidth is:');
32 disp(bandwidth)
33 %% initialisation
34 sigmaL=1/(5*10^(-7));
35 wdetec=1:npix;
36 NH=npix*4; %real spectrum is continuous.
37         %higher spectral resolution for the input is needed.
38 kmin=sigmaL-1.5*bandwidth; %input spectrum has larger bandwidth
39         %than the instrument.
40 kmax=sigmaL+0.5*bandwidth;
41 %% input spectrum
42 % we create a delta_fucion located at the centrum of the bandwidth
43 x=1:NH;
44 y=zeros(size(x));
45 dk=(kmax-kmin)/NH;
46 y(NH/2)=1/(2*dk);
47 y(NH/2+1)=1/(2*dk);
48 kstep=(kmax-kmin)/NH;
49 %% list of wave numbers
50 kvec=kmin+kstep/2:kstep:kmax-kstep/2;
51 disp('minimal input wave number is');
52 disp (kmin/100);
53 disp ('maximal input wave number is');
54 disp (kmax/100);
55 disp ('central values for k are');
56 a=kvec(NH/2);
57 disp(a/100);
58 b=kvec(NH/2+1);
59 disp(b/100);
60 R=ones(size(x)); %spectral transmission of the instrument
61 %% position_vector
62 pos=-L/2+L/(2*npix):L/npix:L/2-L/(2*npix);
63 t=0.5*ones(size(pos));

```

```

64 %% dimensions
65 nk=max(size(kvec));
66 nx=max(size(pos));
67 B_u=y.*R;
68 t_u=2*t.^2;
69 dk=(kmax-kmin)/nk;
70 UM=zeros(nk,nx);
71 Angle=zeros(nk,nx);
72 csang=zeros(nk,nx);
73 for j=1:nx
74     for i=1:nk
75         UM(i,j)=dk*B_u(i)*t_u(j);
76     end;
77 end;
78 %I_u=sum(UM);
79 t_m=2*t.^2;
80 d=tand(thetaL);
81 d=d*8*pi;
82 posang=d*pos;
83 kappa=kvec-sigmaL;
84 M=zeros(nk,nx);
85 MM=zeros(nk,nx);
86 for j=1:nx
87     for i=1:nk
88         M(i,j)=dk*B_u(i)*t_m(j);
89         Angle(i,j)=(kappa(i)*posang(j));
90         csang(i,j)=cos(Angle(i,j));
91         MM(i,j)=csang(i,j)*M(i,j);
92     end;
93 end;
94 %I_m=sum(MM);
95 %figure(1);
96 %plot(pos,I_m+I_u);
97 %legend('total interferogram');
98 %figure(2)
99 %plot(pos,I_u);
100 %legend('unmodulated part');
101 %figure(3)
102 %plot(pos,I_m);
103 %legend('modulated signal');
104 modulated=modulated(kvec,R,y,pos,t,t,thetaL,sigmaL);

```

```

105 unmodulated=unmodulated(kvec,R,y,pos,t,t);
106 total=exoptics(kvec,R,y,pos,t,t,thetaL,sigmaL);
107 figure(1);
108 plot(pos,total);
109 legend('total interferogram');
110 figure(2)
111 plot(pos,unmodulated);
112 legend('unmodulated part');
113 figure(3)
114 plot(pos,modulated);
115 legend('modulated signal');
116 % recover spectrum
117 recov=fliplr(abs(iffshift(iffshift(iffshift(modulated)))));
118 figure(4);
119 plot(kvec(NH/4+1:0.75*NH),y(NH/4+1:0.75*NH));
120 legend('input spectrum');
121 kminout=sigmaL-bandwidth;
122 kmaxout=sigmaL+bandwidth;
123 kstpout=(kmaxout-kminout)/npix;
124
125 kout=kminout+kstpout/2:kstpout:kmaxout-kstpout/2;
126 krec=kout(1:max(size(kout)/2));
127 recspec=recov(1:max(size(recov)/2));
128 figure(5);
129 plot(krec,recspec);
130 legend('recovered spectrum');
131 %% input spectrum
132 % we create a delta_funcion located 1/100th Bandwidth of the Littrow angle
133 x=1:NH;
134 y=zeros(size(x));
135 dk=(kmax-kmin)/NH;
136 y(0.75*NH-0.005*NH)=1/(2*dk);
137 y(0.75*NH-0.005*NH+1)=1/(2*dk);
138 kstep=(kmax-kmin)/NH;
139
140 kvec=kmin+kstep/2:kstep:kmax-kstep/2;
141 disp('minimal input wave number is');
142 disp(kmin/100);
143 disp('maximal input wave number is');
144 disp(kmax/100);
145 disp('spectrum is zero except for wave number difference of');

```

```

146 a=sigmaL-kvec(0.75*NH-0.005*NH+1);
147 disp(a);
148 disp('and wavenumber is')
149 b=kvec(0.75*NH-0.005*NH);
150 disp(b);
151 R=ones(size(x));%spectral transmission of the instrument
152 %% position_vector
153 pos=-L/2+L/(2*npix):L/npix:L/2-L/(2*npix);
154 t=0.5*ones(size(pos));
155 B_u=y.*R;
156 t_u=2*t.^2;
157 dk=(kmax-kmin)/NH;
158 UM=zeros(NH,npix);
159 Angle=zeros(NH,npix);
160 csang=zeros(NH,npix);
161 for j=1:npix
162     for i=1:NH
163         UM(i,j)=dk*B_u(i)*t_u(j);
164     end;
165 end;
166 I_u=sum(UM);
167 t_m=2*t.^2;
168 d=tand(thetaL);
169 d=d*8*pi;
170 posang=d*pos;
171 kappa=kvec-sigmaL;
172 M=zeros(NH,npix);
173 MM=zeros(NH,npix);
174 for j=1:npix
175     for i=1:NH
176         M(i,j)=dk*B_u(i)*t_m(j);
177         Angle(i,j)=((kappa(i))*posang(j));
178         csang(i,j)=cos(Angle(i,j));
179         MM(i,j)=csang(i,j)*M(i,j);
180     end;
181 end;
182 I_m=sum(MM);
183 figure(6);
184 plot(pos,I_m+I_u);
185 legend('total interferogram');
186 figure(7)

```



```

187 plot(pos, I_u);
188 legend('unmodulated part');
189 figure(8)
190 plot(pos, I_m);
191 legend('modulated signal');
192 % recover spectrum
193 recov=fliplr(abs(ifftshift(ifft(ifftshift(I_m))))));
194 figure(9);
195 plot(kvec(NH/4+1:0.75*NH), y(NH/4+1:0.75*NH));
196 legend('input spectrum');
197 kminout=sigmaL-bandwidth;
198 kmaxout=sigmaL+bandwidth;
199 kstpout=(kmaxout-kminout)/npix;
200 kout=kminout+kstpout/2:kstpout:kmaxout-kstpout/2;
201 krec=kout(1:max(size(kout)/2));
202 recspec=recov(1:max(size(recov)/2));
203 figure(10);
204 plot(krec, recspec);
205 legend('recovered spectrum');

```

Doppler Shift in Quasar Disks

doplermain.m

```

1 clc
2 clear all
3 close all
4 %% doppler shift in quasar
5 %% study of FWHM of MgII line
6 %% Define parameters
7 %% samplings for several errors on the littrow wavelength
8 %% are averaged to make the wave number dependent shift correction
9 %% errors are calculated for all the parameters directly linked to the
10 %% littrow wavelength
11
12 k_c=1/((280)*10^-9);
13 BW_min=20*10^-9;
14 npix=2048;
15 NH=4000;

```

```

16 lambda_litt=1/k_c-BW_min/2;
17 Lambda_error=0.01;
18 NS=5; %number of samples
19 sigma_l=1/lambda_litt;
20 R_max=0.5*npix*lambda_litt/BW_min;
21 N_max=R_max/4;
22 N_grating=3200;
23 beam_width=0.02;
24 tanteta=0.5*lambda_litt*N_grating/beam_width;
25 pos=-beam_width/2+beam_width/(2*npix):beam_width/npix:beam_width/2-beam_width/(2*npix);
26 BW=lambda_litt*npix/(8*N_grating);
27
28
29 %% arm A sensitivity
30 fileID = fopen('detec2048_a.txt','r'); %detec 2048 is a text file in wich
31 % a vector of 2048 values between 0.6 and 0.7 are stored, representing the
32 % sensitivity of the detector. The numbers are randomly distributed over
33 % the vector.
34 formatSpec = '%f';
35 sensitivity_a=0.5*(fscanf(fileID,formatSpec));
36 %% arm B sensitivity
37 fileID = fopen('detec2048_b.txt','r'); %detec 2048 is a text file in wich
38 % a vector of 2048 values between 0.6 and 0.7 are stored, representing the
39 % sensitivity of the detector. The numbers are randomly distributed over
40 % the vector.
41 formatSpec = '%f';
42 sensitivity_b=0.5*(fscanf(fileID,formatSpec));
43
44 %% error vector
45 fileID = fopen('sample.txt','r'); %contains an list of deviations from
46 %the nominal Littrow wavelength.
47 formatSpec = '%f';
48 corr_vec=(0.99+Lambda_error*(fscanf(fileID,formatSpec)));
49
50 %% Define input spectrum
51
52 k_max=1/(lambda_litt-BW);
53 k_min=1/(lambda_litt+BW);
54 dk=(k_max-k_min)/NH;
55 kvec=k_min+dk/2:dk:k_max-dk/2;
56

```

```

57 alpha=4/(((6.32)*10^-9))^2;
58 y=2.^(-alpha*(1./kvec-1/k_c).^2);
59 kmin=1/(1/k_c+0.45*BW);
60 kmax=1/(1/k_c-0.45*BW);
61 filter=specfilter(kmin,kmax,kvec);
62 lambda_n=corr_vec*lambda_litt;
63 sigma_n=1./lambda_n;
64 tan_new=corr_vec*tanteta;
65
66 fileID = fopen('wavenum4000.txt','r');
67 formatSpec = '%f';
68 correction=(fscanf(fileID,formatSpec))';
69 y=0.97*y+correction-0.97;
70 y_domain=filter.*y;
71 figure(1)
72 plot(0.01*kvec,y)
73 figure(2)
74 plot(0.01*kvec,filter)
75 figure(3)
76 plot(0.01*kvec,y_domain)
77 y=y_domain;%cut high frequencies
78 %g=0.5*(y+fliplr(y));%symetrize the spectrum
79 %y=g;%use the symmetric spectrum
80 IM = zeros(NS,npix);
81 IU = zeros(NS,npix);
82 IT = zeros(NS,npix);
83 IFF = zeros(NS,npix);
84 IC = zeros(NS,npix);
85 IS= zeros(NS,npix);
86
87 for j=1:NS
88 BW_N=lambda_n(j)*npix/(8*N_grating);
89 k_min=1/(lambda_n(j)+BW_N);
90 k_max=2/(lambda_n(j))-k_min;
91 dk=(k_max-k_min)/NH;
92 kvec=k_min+dk/2:dk:k_max-dk/2;
93
94 %% Modulated part of the output
95 IM(j,:)=modt(kvec, sensitivity_a,sensitivity_b,pos,tan_new(j),y,sigma_n(j),dk);
96 %IM=IM/max(max(IM));
97 figure(4)

```

```

98 plot (pos, IM)
99
100 %% Unmodulated part of the output
101 IU(j, :)=unmodt (y, sensitivity_a, sensitivity_b, dk);
102 %IU=IU/(max(max(IU)));
103 figure(5)
104 plot (pos, IU)
105
106 %% Total detected signal
107 IT(j, :)=Iout (kvec, sensitivity_a, sensitivity_b, pos, tan_new(j), y, sigma_n(j), dk);
108 %IT=IT/max(max(IT));
109 figure(6)
110 plot (pos, IT)
111
112 %% Flat field corrected signal
113 IFF(j, :)=flat (IM(j, :), sensitivity_a, sensitivity_b);
114 %IFF=IFF/max(max(IFF));
115 figure(7)
116 plot (pos, IFF)
117
118 IS(j, :)=shift_corr (IFF(j, :));
119
120 %% cosine for contributions of each measurement
121 IC(j, :)=coscoeff (sigma_n(j), pos, tan_new, sigma_l);
122 end
123 %%
124 %% contribution for each sample measurement
125 %%
126 IMOD=sum (IM) /NS;
127 figure(8)
128 plot (pos, IMOD)
129
130 IUNMOD=sum (IU) /NS;
131 figure(9)
132 plot (pos, IUNMOD)
133
134 ITOT=sum (IT) /NS;
135 figure(10)
136 plot (pos, ITOT)
137
138 IFFfield=sum (IFF) /NS;

```

```

139 figure(11)
140 plot(pos,IFField)
141
142 I_shift=sum(IS)/NS;
143 figure(12)
144 plot(pos,I_shift)
145
146 %% Spectrum Recovery
147 k_min=1/(lambda_litt+BW);
148 k_max=2*sigma_l-k_min;
149
150 I_treat= 0.5*(IFField+fliplr(IFField));
151 kmaxout=sigma_l-k_min;
152 kminout=sigma_l-k_max;
153 sintetan=0.5*lambda_litt*npix/beam_width;
154 teta=asin(sintetan);
155 kstp=(kmaxout-kminout)/npix;
156 recov=cos(teta)/kstp*(abs(iffshift(iffshift(iffshift(I_treat))))));
157 recov=0.5*recov+0.5*fliplr(recov);
158 kout=kminout+kstp/2:kstp:kmaxout-kstp/2;
159
160 %% the recovered spectrum is given for a two times less accurate
161 %% precision than the input, because the spectrum does not make difference
162 %% between wavenumbers greater or lower than Littrow
163
164 kappa_rec=2*kout;
165 figure(13)
166 plot(2*kout, recov);
167 legend('recovered for unbalanced arms')
168 figure(14)
169 plot(kvec, filter)
170 k_final=kappa_rec((npix/4+1):npix/2);
171 coeff=max(max(k_final))-min(min(k_final))/max(size(k_final));
172 recov_final=(recov((npix/4+1):npix/2));
173 recov_final=recov_final*max(y)/max(recov_final);
174 figure(15)
175 plot(k_final+sigma_l, recov_final);
176 cos(teta)

```

bandpass filter

```

1 function output=specfilter(kmin,kmax,kvec)
2 N=max(size(kvec));
3 R=(kmax-kmin)/(max(max(kvec))-min(min(kvec)));
4 dk=(kmax-kmin)/(N*R);
5
6 output=1/pi*(atan((kvec-kmin)/dk)-atan((kvec-kmax)/dk));

```

function that calculates the modulated part

```

1 function output=modt(wavevec, ta,tb,pos,tanteta,y,sigma,dk)
2 tm=2*ta.*tb;
3 wavevec=sigma-wavevec;
4 Kappa=wavevec*4*tanteta;
5 M=dk*y'*tm;
6 A=2*pi*Kappa'*pos;
7 A=cos(A);
8 MM=M.*A;
9 output=sum(MM);

```

function that calculates the unmodulated part

```

1 function output=unmodt(y,ta,tb,dk)
2 tu=(ta.^2+tb.^2);
3 U=dk*y'*tu;
4 output=sum(U);

```

function that calculates the interferogram

```

1 function output=Iout(wavevec, ta,tb,pos,tanteta,y,sigma,dk)
2 tm=ta.*tb;
3 wavevec=wavevec-sigma;
4 pos=8*pi*tanteta*pos;
5 M=dk*y'*tm;
6 A=wavevec'*pos;
7 A=cos(A);
8 MM=M.*A;
9 tu=0.5*(ta.^2+tb.^2);
10 U=dk*y'*tu;
11 output=sum(MM)+sum(U);

```

function that calculates the flat field correction

```
1 function output=flat (I_m,t_a,t_b)
2 t_cross=2*t_a.*t_b;
3 IC_m=I_m./t_cross;
4 output=IC_m;
```

function that calculates the weight of all the samples

```
1 function output=coscoeff (wavevec,pos,tanteta,sigma)
2 wavevec=sigma-wavevec;
3 Kappa=wavevec*4*tanteta;
4 A=2*pi*Kappa'*pos;
5 A=cos (A) ;
6 output=sum (A) ;
```

Mars Atmospheric Water Lines

marsmain.m

```
1 clc
2 clear all
3 close all
4 %% Study of the atmospheric water of mars
5 %% entrance and exit optics temperatures
6 T_sun=5100;
7 omega_sun=4*10^(-5);
8 temp_in=150;
9 temp_out=120;
10 calibration_emissivity=0.9;
11 omega_syst=0.18;
12 %% calibration black bodies temperatures
13 T_H=155;
14 T_C=145;
15 %% speed of light
16 c=3*10^8;
```

```

17 %% Planck constant
18 h=6.26*10^(-34);
19 %% input wavenumbers
20 x=301001:319000;
21 %% Preparation of the input spectrum (negative Peaks are manually added to the...
22 %%...signal, in order to
23 %% reproduce spectracl absorbtion rays)
24 y_in=ones(size(x));
25 y_in((301550-75-301250):(301550+75-301250))=1-0.02*(cos(pi*(x((301550-75-301250):...
26 ... (301550+75-301250))-301550-301250)/150)).^4;
27 y_in((302200-75-301250):(302200+75-301250))=1-0.011*(cos(pi*(x((302200-75-301250):...
28 ... (302200+75-301250))-302200-301250)/150)).^4;
29 y_in((302600-75-301250):(302600+75-301250))=1-0.04*(cos(pi*(x((302600-75-301250):...
30 ... (302600+75-301250))-302600-301250)/150)).^4;
31 y_in((303050-75-301250):(303050+75-301250))=1-0.041*(cos(pi*(x((303050-75-301250):...
32 ... (303050+75-301250))-305050-301250)/150)).^4;
33 y_in((303190-75-301250):(303190+75-301250))=1-0.027*(cos(pi*(x((303190-75-301250):...
34 ... (303190+75-301250))-303190-301250)/150)).^4;
35 y_in((303220-75-301250):(303220+75-301250))=1-0.029*(cos(pi*(x((303220-75-301250):...
36 ... (303220+75-301250))-303220-301250)/150)).^4;
37 y_in((303400-75-301250):(303400+75-301250))=1-0.042*(cos(pi*(x((303400-75-301250):...
38 ... (303400+75-301250))-303400-301250)/150)).^4;
39 y_in((303500-75-301250):(303500+75-301250))=1-0.013*(cos(pi*(x((303500-75-301250):...
40 ... (303500+75-301250))-303500-301250)/150)).^4;
41 y_in((304850-75-301250):(304850+75-301250))=1-0.022*(cos(pi*(x((304850-75-301250):...
42 ... (304850+75-301250))-304850-301250)/150)).^4;
43 y_in((304900-75-301250):(304900+75-301250))=1-0.003*(cos(pi*(x((304900-75-301250):...
44 ... (304900+75-301250))-304900-301250)/150)).^4;
45 y_in((305700-75-301250):(305700+75-301250))=1-0.046*(cos(pi*(x((305700-75-301250):...
46 ... (305700+75-301250))-305700-301250)/150)).^4;
47 y_in((306000-75-301250):(306000+75-301250))=1-0.04*(cos(pi*(x((306000-75-301250):...
48 ... (306000+75-301250))-306000-301250)/150)).^4;
49 figure(1)
50 y_in=y_in.^12;
51 plot(x/100,y_in)
52 %% entrance optics
53 y_inp=omega_sun*Planck(T_sun,x).*y_in+Planck(temp_in,x);
54 %% define parameters
55 npix=1024;
56 NH=4000;
57 lambda_litt_esti=1/306250;

```



```

58 lambda_litt=3.24*10^(-6);
59 Lambda_error=0.01;
60 BW_min=(1/301350)-lambda_litt;
61 sigma_l=1/lambda_litt;
62 R_max=0.5*npix*lambda_litt/BW_min;
63 N_max=R_max/4;
64 N_grating=5120;
65 beam_width=0.032;
66 tanteta=0.5*lambda_litt*N_grating/beam_width;
67 BW=lambda_litt*npix/(8*N_grating);
68 k_min_input=1/(lambda_litt+BW); %% 301114 (inside the input wavenumbers-->OK
69 pos=-beam_width/2+beam_width/(2*npix):beam_width/npix:beam_width/2-beam_width...
70 .../(2*npix);
71 %% arm A sensitivity
72 fileID = fopen('detec1024_a.txt','r'); %detec 1024 is a text file in wich
73 % a vector of 1024 values between 0.6 and 0.7 are stored, representing the
74 % sensitivity of the detector. The numbers are randomly distributed over
75 % the vector.
76 formatSpec = '%f';
77 sensitivity_a=0.5*(fscanf(fileID,formatSpec));
78 %% arm B sensitivity
79 fileID = fopen('detec1024_b.txt','r'); %detec 1024 is a text file in wich
80 % a vector of 1024 values between 0.6 and 0.7 are stored, representing the
81 % sensitivity of the detector. The numbers are randomly distributed over
82 % the vector.
83 formatSpec = '%f';
84 sensitivity_b=0.5*(fscanf(fileID,formatSpec));
85 %% resample spectrum
86 k_min=1/(lambda_litt+BW);
87 k_max=2*sigma_l-k_min;
88 dk=(k_max-k_min)/NH;
89 kvec=k_min+dk/2:dk:k_max-dk/2;
90 y = interp1(x,y_inp,kvec);
91 %% calibration black bodies
92 cal_h=Planck(T_H,kvec);
93 cal_c=Planck(T_C,kvec);
94 kmin=1/(lambda_litt+1.05*BW);
95 kmax=sigma_l;
96 filter=specfilter(kmin,kmax,kvec);
97 y_domain=filter.*y;
98 g=0.5*(y_domain+fliplr(y_domain));%symetrize the spectrum

```

```

99 y=g;%use the symetric spectrum
100 figure(2)
101 plot(kvec,y);
102 figure(3)
103 plot(0.01*kvec,y_domain)
104
105 cal_hot_m=modt(kvec,sensitivity_a,sensitivity_b,pos,tanteta,filter.*cal_h,...
106 ...sigma_l,dk);
107 cal_hot_u=unmodulated(filter.*cal_h,sensitivity_a,sensitivity_b,dk,temp_out,kvec);
108
109 hot_a=unmodulated(filter.*cal_h,2*sensitivity_a,0,dk,temp_out,kvec);
110 hot_b=unmodulated(filter.*cal_h,0,2*sensitivity_b,dk,temp_out,kvec);
111
112 hot_corr=0.5*sqrt(hot_a.*hot_b)/(0.5*(hot_a+hot_b));
113
114 cal_cold_m=modt(kvec,sensitivity_a,sensitivity_b,pos,tanteta,filter.*cal_c,...
115 ...sigma_l,dk);
116 cal_cold_u=unmodulated(filter.*cal_c,sensitivity_a,sensitivity_b,dk,temp_out,kvec);
117
118 cold_a=unmodulated(filter.*cal_c,2*sensitivity_a,0,dk,temp_out,kvec);
119 cold_b=unmodulated(filter.*cal_c,0,2*sensitivity_b,dk,temp_out,kvec);
120
121 cold_corr=0.5*sqrt(cold_a.*cold_b)/(0.5*(cold_a+cold_b));
122
123 cal_hot=modt(kvec,sensitivity_a,sensitivity_b,pos,tanteta,filter.*cal_h,sigma_l,...
124 ...dk)./hot_corr;
125 cal_cold=modt(kvec,sensitivity_a,sensitivity_b,pos,tanteta,filter.*cal_c,sigma_l,...
126 ...dk)./cold_corr;
127
128 cal_hot=shift_corr(cal_hot);
129 cal_cold=shift_corr(cal_cold);
130 %% Modulated part of the output
131 IMOD=modt(kvec,sensitivity_a,sensitivity_b,pos,tanteta,y,sigma_l,dk);
132 %IM=IM/max(max(IM));
133 figure(4)
134 plot(pos,IMOD)
135 %% Unmodulated part of the output
136 IUNMOD=unmodulated(y,sensitivity_a,sensitivity_b,dk,temp_out,kvec);
137 I_a=unmodulated(y,2*sensitivity_a,0,dk,temp_out,kvec);
138 I_b=unmodulated(y,0,2*sensitivity_b,dk,temp_out,kvec);
139 flat_corr=0.5*sqrt(I_a.*I_b)/(0.5*(I_a+I_b));

```

```

140 %IU=IU/(max(max(IU)));
141 figure(5)
142 plot(pos,IUNMOD)
143 %% Total detected signal
144 ITOT=Iout(kvec, sensitivity_a,sensitivity_b,pos,tanteta,y,sigma_l,dk);
145 %IT=IT/max(max(IT));
146 figure(6)
147 plot(pos,ITOT)
148 %% Flat field corrected signal
149 IFField=IMOD./flat_corr;
150 %IFF=IFF/max(max(IFF));
151 figure(7)
152 plot(pos,IFField)
153 I_shift=shift_corr(IFField);
154 figure(12)
155 plot(pos,I_shift)
156 %% Spectrum Recovery
157 k_min=1/(lambda_litt+BW);
158 k_max=2*sigma_l-k_min;
159 I_treat= 0.5*(I_shift+fliplr(I_shift));
160 hot_treat=0.5*(cal_hot+fliplr(cal_hot));
161 cold_treat= 0.5*(cal_cold+fliplr(cal_cold));
162 kmaxout=sigma_l-k_min;
163 kminout=sigma_l-k_max;
164 teta=atan(tanteta);
165 kstp=(kmaxout-kminout)/npix;
166 recov=(cos(teta)/kstp)*(abs(ifftshift(ifft(ifftshift(I_treat)))));
167 recov=0.5*recov+0.5*fliplr(recov);
168 kout=kminout+kstp/2:kstp:kmaxout-kstp/2;
169 recov_h=(cos(teta)/kstp)*(abs(ifftshift(ifft(ifftshift(hot_treat)))));
170 recov_c=(cos(teta)/kstp)*(abs(ifftshift(ifft(ifftshift(cold_treat)))));
171 %% the recovered spectrum is given for a two times less accurate
172 %% precision than the input, because the spectrum does not make difference
173 %% between wavenumbers greater or lower than Littrow
174 kappa_rec=2*kout;
175 figure(13)
176 plot(2*kout,recov);
177 legend('recovered for unbalanced arms')
178 figure(14)
179 plot(kvec,filter)
180 k_final=kappa_rec((npix/4+1):npix/2);

```

```

181 coeff=max(max(k_final))-min(min(k_final))/max(size(k_final));
182 recov_final=(recov((npix/4+1):npix/2));
183 %h_cal=(recov_h((npix/4+1):npix/2));
184 %c_cal=(recov_c((npix/4+1):npix/2));
185 %h_in=interp1(kvec,cal_h,k_final+sigma_l);
186 %c_in=interp1(kvec,cal_c,k_final+sigma_l);
187 %r=(h_cal-c_cal)./(h_in-c_in);
188 %g=(h_cal./r-h_in);
189 %recov_final=recov_final./r-g;
190 recov_final=recov_final./(omega_sun*Planck(T_sun,k_final+sigma_l));
191 h_cal=(recov_h((npix/4+1):npix/2));
192 c_cal=(recov_c((npix/4+1):npix/2));
193 h_in=interp1(kvec,cal_h,k_final+sigma_l);
194 c_in=interp1(kvec,cal_c,k_final+sigma_l);
195 r=(h_cal-c_cal)./(h_in-c_in);
196 g=(h_cal./r-h_in);
197 recov_final=recov_final./r-g;
198 figure(15)
199 plot(k_final+sigma_l,recov_final);
200 figure(16)
201 plot(x,y_in)
202
203 %% Noise model
204 %% For the model, I took similar orders of values than proposed in the
205 %% thesis of Perkins
206 %% Since the principal source of noise is the shot noise, I thought that
207 %% studying for different integration times the average SNR could be an interesting
208 %% point for the work here presented
209 % additional parameters
210 % pixel area
211 A_pix=4*10^(-10);
212 % integration time
213 t_int=1/500;
214 % Quantum efficiency
215 Qeff=0.7;
216 % fram rate
217 rate= 50; %frame/sec
218 %calibration error rate
219 cal_e=0.0001;
220 %specific detectivity
221 Dstar=10^12; %W/m/sqrt(Hz)

```

```

222 %system aperture Area
223 Aa=9*10^(-4);
224 %Noise Power Spectral Density
225 NPSD=10^-7; %V/sqrt(Hz)
226 %Responsivity
227 Res=100; %V/W
228 bits=20;
229 bit_error=10^(-9);
230 %conversion coefficients
231 %spectral radiance -> number of electrons
232 C1=((k_max-k_min)*A_pix*omega_sun*t_int*Qeff)/(h*c*(k_final+sigma_1));
233 %irradiance->number of electrons
234 C2=(A_pix*omega_sun*t_int*Qeff)/(h*c*mean(k_final+sigma_1));
235 %k-noise->x-noise
236 C3=sqrt(2/max(size(k_final)))*2;
237 %Interferogram number of electrons
238 signal_e=ITOT.*C2;
239 % saturation
240 sat=1.2*max(max(signal_e));
241 %interferogram domain
242 shot_noise=mean(sqrt(signal_e));
243 cal_noise=cal_e*(shot_noise).^2;
244 %spectral domain
245 det_noise=mean(2/(Aa*omega_sun*2*kstp*Dstar))*sqrt(A_pix*rate)/mean((sensitivity_a...
246 ...+sensitivity_b)/2).*C1;
247 el_noise=mean(4*beam_width/2*NPSD*sqrt(rate)/(Aa*omega_sun*Res)/mean((sensitivity_a...
248 ...+sensitivity_b)/2).*C1;
249 quant_noise=mean(sat/(sqrt(12)*2^(bits)-1).*C1);
250 bit_noise=0;
251 for q= 0:bits-1;
252     bit_noise=bit_noise+(2^q*(sat./C1)/(2^bits-1)).^2;
253 end
254 bit_noise=mean(sqrt(bit_error/bits*bit_noise).*C1);
255 total_noise=sqrt((shot_noise*C3).^2+(cal_noise*C3).^2+(det_noise).^2+...
256 ...+(el_noise).^2+(quant_noise).^2+(bit_noise).^2);
257 NESR=(total_noise).*C1.^(-1)/mean(Planck(T_sun,k_final+sigma_1));
258 SNR=recov_final./NESR;
259 figure(18)
260 plot(k_final+sigma_1,SNR);

```

bandpass filter

```

1 function output=specfilter(kmin,kmax,kvec)
2 N=max(size(kvec));
3 R=(kmax-kmin)/(max(max(kvec))-min(min(kvec)));
4 dk=(kmax-kmin)/(N*R);
5
6 output=1/pi*(atan((kvec-kmin)/dk)-atan((kvec-kmax)/dk));

```

function that calculates the modulated part

```

1 function output=specfilter(kmin,kmax,kvec)
2 N=max(size(kvec));
3 R=(kmax-kmin)/(max(max(kvec))-min(min(kvec)));
4 dk=(kmax-kmin)/(N*R);
5
6 output=1/pi*(atan((kvec-kmin)/dk)-atan((kvec-kmax)/dk));

```

function that calculates the unmodulated part

```

1 function output=unmodulated(y,ta,tb,dk,Tout,kvec)
2 tu=(ta.^2+tb.^2);
3 U=dk*y'*tu+Planck(Tout,kvec)'*ones(size(tu));
4 output=sum(U);

```

Bibliography

- [1] Perkins Cara. Spatial heterodyne spectroscopy: Modeling and interferogram processing. <<https://scholarworks.rit.edu/theses/1062/>>, 2013. [Online; accessed 03-January-2021].
- [2] Bozena Czerny Conor Wildy. The relationship between mgii broad emission and quasar inclination angle. *Frontiers in Astronomy and Space Sciences*, 4(43):1–7, 2017.
- [3] JASON DETWILER. *PHYSIC 331A Lecture5: Fourier Spectroscopy, Fabry-Perot Interferometers, and Lasers*, (2013).
- [4] Harlander John M. Englert Christoph R. Flatfielding in spatial heterodyne spectroscopy. *Applied Optics*, 45(19):4583–4590, 2006.
- [5] Gornushkin Igor B. et al. Laser-induced breakdown spectroscopy combined with spatial heterodyne spectroscopy. *Applied Spectroscopy*, 68(9):1076–1074, 2014.
- [6] Jeffrey Langille et al. Spatial heterodyne observation of water (show) from a high-altitude airplane: characterization, performance, and first results. *Copernicus Publications, Atmos Meas. Tech*, 431(12):431–455, 2019.
- [7] Jilin Liu et al. Analysis and correction of distortions in spatial heterodyne spectrometer system. *Applied Optics*, 58(9):2190–2197, 2019.
- [8] Sona Hosseinia. Khayyam; progress and prospects of coupling a spatial heterodyne spectrometer (shs) to a cassegrain telescope for optical interferometry. <<http://trjs.jpl.nasa.gov/>>, 2016. [Online; accessed 03-January-2021].
- [9] <http://www.mathworks.com/matlabcentral/fileexchange/8015>. *How to insert MATLAB code into LaTeX*, (2013).
- [10] Nirmal Kaipachery. Design and modeling of a tunable spatial heterodyne spectrometer for emission line studies. arXiv:1804.09358v2 [astro-ph.IM] 26 Apr 2018, 2018. [Online; accessed 03-January-2021].

- [11] Jean-Claude Diels Matthias Lenzner. Concerning the spatial heterodyne spectrometer. *Optical Society of America*, 24(2):1829–1839, 2016.
- [12] Gregg A Swayze et al. Roger N. Clark. Spectroscopy from space. *Reviews in Mineralogy and Chemistry*, 78(9):399–446, 2014.